Relationships between magmatism and extension along the Autun-La Serre fault system in the Variscan Belt of the eastern French Massif Central

Flavien Choulet, Michel Faure, Olivier Fabbri, Patrick Monié

Relationships between magmatism and extension along the Autun - La Serre fault system in the Variscan Belt of the eastern French Massif Central

Flavien Choulet [1,*], Michel Faure [1], Olivier Fabbri [2], Patrick Monié [3]

[1] ISTO, UMR 6113 - CNRS/Université d'Orléans, 1A, rue de la Férollerie, 45071 Orléans Cedex 2, France

[2] Chrono-environnement, UMR 6249 – Université de Franche-Comté, 16, route de Gray 25030 Besançon Cedex, France

[3] Géosciences Montpellier, UMR CNRS 5243, Université Montpellier II, Place Bataillon, 34095 Montpellier Cedex 5, France

Corresponding author

flavien.choulet@univ-orleans.fr, +33238492573

Abstract

The ENE-WSW Autun Shear Zone, in the northeastern part of the French Massif Central has been interpreted previously as a dextral wrench fault. New field observations and microstructural analyses document a NE-SW stretching lineation that indicates normal dextral motions along this shear zone. Further east, similar structures are observed along the La Serre Shear Zone. In both areas, a strain gradient from leucogranites with a weak preferred orientation to highly sheared mylonites supports a continuous Autun-La Serre fault system. Microstructural observations and shape and lattice preferred orientation document high-temperature deformation and magmatic fabrics in the Autun and La Serre granites, whereas low- to intermediate-temperature fabrics characterize the mylonitic granite. Electron microprobe monazite geochronology of the Autun and La Serre granites yields a ca. 320 Ma age for pluton emplacement, while mica ^{40}Ar-^{39}Ar datings of the Autun granite yield plateau ages from 305 to 300 Ma. The ca. 300 Ma ^{40}Ar-^{39}Ar ages, obtained on micas from Autun and La Serre mylonites, indicate the time of the mylonitization. The ca. 15 Ma time gap between pluton emplacement and deformation along the Autun-La Serre fault system argue against a synkinematic pluton emplacement during late-orogenic to post-orogenic extension of the Variscan Belt. A ductile to brittle continuum of deformation is observed along the shear zone, with Lower Permian brittle faults controlling the development of sedimentary basins. These results suggest a two-stage Late Carboniferous extension in the northeastern French Massif Central, with regional crustal melting and emplacement of the Autun and La Serre leucogranites around 320 Ma, followed, at 305-295 Ma, by ductile shearing, normal brittle faulting, and subsequent exhumation along the Autun –La Serre transtensional fault system.

Keywords: Variscan Belt, Late Carboniferous shear zones, synkinematic granite, ^{40}Ar-^{39}Ar dating, electron microprobe monazite dating, quartz c-axis, French Massif Central.

1. Introduction

Continental collision leads to the thrusting of two lithospheric plates and a subsequent crustal thickening during orogen formation. Once the lithostatic and compressional strengths are no longer balanced, the orogen becomes unstable and collapses (e.g. Malavieille 1987; Dewey 1988). The gravitational collapse of the thickened crust is accommodated by extension and is characterized by thermal relaxation inducing partial melting of the continental crust (England and Thompson 1986). S-type magmatism, granite-gneiss domes and normal shear zones document syn to post-orogenic extension (Reynolds and Spencer 1985; McClay et al. 1986; Norton 1986).

Extensional stuctures have also been described in the European Variscan Belt, a large Paleozoic orogen interpreted as the result of the collision between Laurussia, Gondwana, and several intermediate microcontinents such as Armorica or Avalonia (Matte 1986; 2001; Franke 1989). In the French Massif central, one of the main pieces of the Variscan orogen, successive phases of nappe stacking in Devonian and Early Carboniferous times (Burg and Matte 1978; Ledru et al. 1989) led to an important thickening of the crust, and were followed by an important episode of crustal melting (Duthou et al. 1984). During the Late Carboniferous, the collapse of the Variscan Belt (Ménard and Molnar 1988; Burg et al. 1994; Faure 1995) generated normal brittle faults (Echtler and Malavieille 1990; Faure and Becq-Giraudon 1993), normal ductile shear zones (Mattauer et al. 1988; Malavieille et al. 1990), synkinematic granitoids (Faure and Pons 1991; Talbot et al. 2004; Joly et al. 2009), and granite-gneiss domes (Ledru et al. 2001). Although the timing of these events is relatively well established (Faure 1995), the connection between magmatism and extensional tectonics is not always clear. A common idea is that most of the plutons are synkinematic bodies emplaced along normal or strike-slip faults (Faure and Pons 1991; Faure 1995).

This study deals with extensional structures documented by field observations, microstructural analysis, and geochronology of granitoids and mylonites. We focus on the Morvan and La Serre horsts in the northeastern part of the French Massif Central, where S-type granites, ductile shear zones, and syn-sedimentary faults are exposed. We propose an interpretation of the late orogenic to post-orogenic evolution of this segment of the Variscan Belt. We shall use the classical chronostratigraphic stages of Western Europe for the Late Paleozoic period, with Namurian corresponding to Late Mississipian - Early Pennsylvanian (326-313 Ma), Westphalian to Middle Pennsylvanian (313-307 Ma), Stephanian to Late Pennsylvanian (307-303 Ma), Autunian to Late Pennsylvanian - Middle Cisuralian (303-276 Ma), and Saxonian to Late Cisuralian - Middle Guadalupian (276-263 Ma) (Ogg et al. 2008).

2. Geological outline

2.1. The French Massif Central in the Variscan Belt

Two types of scenario have been proposed to account for the geodynamical evolution of the Variscan Belt of Western Europe. The first type is monocyclic and is based on a continuous Paleozoic convergence between Gondwana and Laurussia (Matte 1991; Lardeaux et al. 2001). Alternatively, a polycyclic evolution with two successive orogenic episodes was proposed (Pin 1990; Faure et al. 1997). The reliability of the two scenarios is extensively discussed in several papers (e.g. Faure et al. 2005) and will not be addressed here. In this contribution, the polycyclic scenario is retained. In this model, the first cycle resulted from the Silurian north-directed subduction of the ocean that separated Gondwana and Armorica. After an earlier high-pressure event dated at ca. 415 Ma (Pin and Peucat 1986; Lardeaux et al., 2001), crustal nappes were stacked towards the SW, then partly migmatized, and finally exhumed during the Devonian around 390-380 Ma (Floc'h 1983; Quenardel and Rolin 1984; Roig and Faure 2000; Faure et al. 2008). The second cycle was related to the closure of the Rheic Ocean that initially separated Laurussia and the Armorica microplate (Faure et al. 1997). A Devonian to Early Carboniferous calk-alcaline magmatic suite (Pin et al. 1982) and the Devonian Brévenne ophiolite (Leloix et al. 1999) are interpreted as remnants of a magmatic arc and a back-arc basin related to the southward subduction of the Rheic Ocean (Faure et al. 1997).

During mid-Carboniferous times (Visean), the southern part of the Massif Central experienced top-to-the south nappe stacking, while synorogenic extension prevailed in the north. Late Visean magmatic series, locally called "Tufs Anthracifères", postdate the mid-Carboniferous events (Faure et al. 2002). The Late orogenic stage is characterized by two successive events (Faure and Becq-Giraudon 1993; Burg et al. 1994; Faure 1995): a

Namurian to Westphalian NW-SE extension characterized by leucogranite emplacement (Faure and Pons 1991), followed by a Stephanian to Permian NE-SW extension characterized by brittle normal faulting and formation of coal-bearing half-grabens (Arthaud and Matte 1977; Echtler and Malavieille 1990; Malavieille et al. 1990). Whatever the geodynamic scenario (monocyclic or polycyclic), the Late Carboniferous syn-orogenic to post-orogenic extension is widely accepted,.

2.2. The northeastern French Massif Central

The study area is located in the northeastern French Massif Central, also called Morvan area, which forms a horst between the Cenozoic Limagne and Bresse grabens (Fig. 1). Paleozoic metamorphic units are unconformably overlain by Devonian to Early Carboniferous sedimentary and magmatic rocks (Delfour 1989; Faure et al. 1997) and are crosscut by Carboniferous magmatic intrusions with varied geochemical characteristics (Rolin and Stussi 1991). The last manifestation of this magmatic event is the emplacement of peraluminous plutons such as the Autun granite (Chévremont et al. 1999; Fig. 2a), located close to ductile shear zones in the Autun and Avallon areas (Rolin and Stussi, 1991). Late orogenic brittle wrench or normal faults controlled the development of the Stephanian to Permian coal-bearing half-grabens or pull-apart basins such as the Autun, Epinac or Le Creusot basins (Marteau 1983; Vallé et al. 1988; Fig. 1). These intramontane basins are characterized by a terrigeneous sedimentation, which started during the Late Stephanian and remained active during the Permian (Courel 2001). Stephanian to Permian high-K acidic volcanism is also reported (Carpena et al. 1987; Chévremont et al. 1999).

East of the Oligocene Bresse graben, and close to the northern end of the Jura fold-and-thrust belt, the La Serre horst displays structures similar to those of the Autun area (Fig.

3), with a leucogranitic pluton separated from a Permian sedimentary basin by a ductile shear zone and a brittle fault system (Coromina and Fabbri 2004).

3. Petrography and structure of the studied rocks

3.1. Field data

In the Autun area (Fig. 2a), a N70°E-trending, 500 m wide, mylonitic belt separates Variscan migmatites and granites to the south from a Stephanian to Autunian coal basin to the north (Delfour et al. 1991; Rolin and Stussi 1991). The Autun leucogranite (Fig. 4a) intruded pre-Carboniferous gneisses and migmatites. A porphyritic facies of this leucogranite can be observed in some places. At the hand sample scale, this granite locally shows a planar preferred orientation of biotite and muscovite, and a linear preferred orientation, indicated by K-feldspar and biotite aggregates. However, given the scarcity of outcrops, it is difficult to draw a structural map of the whole pluton (Fig. 2a). To the north, the granitic rocks are more deformed, and the magmatic foliation is reoriented and changed to a tectonic foliation (Fig 2a; b). This change suggests that either the deformation might have occurred during the last stages of pluton emplacement, or that the granitic pluton experienced a post-solidus ductile deformation along the Autun fault. The mylonitization affects all the Variscan rocks, which then display a N60°E to N80°E striking foliation that dips 45° to 80° to the north; a stretching lineation trends N45°E and plunges to the NE (Fig. 2c). Macroscopic shear criteria indicate a top-to-the-NE motion. Shearing was oblique combining strike-slip and dip-slip components (Fig. 4b), not in agreement with previous results on the Autun Shear Zone for which a pure dextral strike-slip faulting was postulated (Rolin and Stussi 1991). North of the shear zone, the mylonites are unconformably overlain by Permian deposits. However, north of Morlet (Fig. 2a), the contact between mylonites to the south and gneiss to the north is a brittle fault hidden westward beneath onlapping Permian deposits (Fig. 2b). Cataclastic mylonitic granites and silicified tectonic breccia, exposed at the southern border of the sedimentary basin, indicate brittle deformation. In the northern part of the Autun basin, the Permian strata overlie Stephanian strata (Marteau 1983; Chévremont et al. 1999) The Autun basin has been described as either a half-graben bounded by normal faults, or a pull-apart basin associated with left-lateral faults (Marteau 1983). The continental deposits composed of conglomerates and sandstones interlayerd with volcanic deposits (Carpena et al. 1987; Chévremont et al. 1999) yielded an Autunian to Saxonian flora described by Bergeron (1889) who defined the Autunian stratotype. Sedimentary filling of this intramontane basin (Courel 2001) is coeval with the activity along the normal boundary fault.

Similar structures are observed in the La Serre area (Fig 3a). A two-mica granite (Morre-Biot 1969) with a weak mica preferred orientation is progressively deformed along the N50°E-trending La Serre Shear Zone, characterized by a N50°E-striking and 60°- to 80°-northwest-dipping mylonitic foliation and a N30°E-trending stretching lineation (Coromina and Fabbri 2004; Fig. 3b). In thin sections, perpendicular to the foliation and parallel to the lineation (XZ sections), sigmoidal muscovites, shear bands and asymmetric porphyroclasts indicate a top-to-the-NE shear sense. To the northwest, the mylonitic belt is limited by the N70°E- to N80°E striking, low angle La Serre Median Brittle Fault, marked by a silicified volcanic breccia (Coromina and Fabbri 2004; Fig 3c). This breccia is similar to the silicified breccia exposed along the Autun shear zone. North of the La Serre Median Brittle Fault, Permian conglomerates and sandstones, with an Upper Autunian to Saxonian continental flora are about 500 m thick (Campy et al. 1983). The La Serre Median Brittle Fault is postdated by flat lying deposits, but it was probably moderately reactivated as a normal fault during the Oligocene extensional tectonics of the Bresse graben and as a reverse fault during Alpine shortening (Coromina and Fabbri 2004; Madritsch et al. 2008).

3.2. Microstructures, shape and lattice preferred orientation analyses

In order to understand the mechanisms of deformation of the Autun and La Serre leucogranites, the rock fabric was studied by several methods. The evolution from a magmatic planar fabric to a tectonic foliation was investigated by relying on mica preferred orientation. Since rock fabric is not well defined, especially in apparently undeformed granites, systematic manual measurements of the orientation of longitudinal sections of muscovite and biotite platelets were carried out in the three principal planes of the strain ellipsoid (XY, XZ and YZ). These planes were estimated from field observations. Manual measurements were also supported by an automatic method using the “SPO” software (Launeau and Robin 2005). On thin section images, each mica was handled as an isolated grain (Fig. 5). The orientation of each grain was computed by using the intercept method, with measurements shown in rose diagrams (Fig. 5). There are no significant differences between manual and automatic procedures. Quartz lattice-preferred orientation (LPO) analysis provides information about deformation mechanisms, glide systems, and activation temperature. Quartz c-axis orientation (Fig. 6) was studied with an U-stage.

3.2.1. Magmatic microstructures

In the two samples of undeformed granite (AU16 and AU19, Fig. 5), a planar fabric can be inferred from the orientation of mica flakes along the XZ and YZ sections. A linear fabric visible along XY sections is better developed in sample AU16 than in sample AU19. Coarse angular quartz grains show seriate to polygonal textures (Moore 1970). Quartz grains display a chessboard pattern of subgrain boundaries (Fig. 4c). Myrmekite is also observed (Fig. 4d) and could indicate a syn-magmatic deformation (Hibbard 1987), although myrmekitic textures can also develop under solid-state conditions (Simpson et Wintsch 1989).

In samples from the undeformed Autun and La Serre granites (AU16, AU19, AU28, AU29 and SE03, Fig. 6), c-axis maxima in the XZ plane are observed at 0 to 45° from the X axis of the finite strain. Such a c-axis distribution is typical of prism <c> slip and is representative of high-temperature deformation mechanisms (Mainprice et al. 1986). Nevertheless, the chessboard textures observed in the two plutons indicate either a combined basal <a> and prism <c> slip (Mainprice et al. 1986; Stipp et al. 2002), or the transition from low-temperature to high-temperature quartz (Kruhl 1996). Whatever the mechanism is, and considering that no fluids have caused a late recrystallization, microstructures in undeformed granite reveal high temperature of deformation of ca. 700°C, close to the magma crystallization (Kruhl 1996).

3.2.2. Low-temperature mylonite deformation

In the two samples of mylonitic granite (AU02 and AU20, Fig. 5), well-defined maxima in the rose diagram correspond to the rock planar fabric. The bimodal orientation of micas probably correlates with distinct shear bands and recrystallization of mica. In the mylonitic granite, microstructures are characteristic of ductile deformation with shear bands crosscutting a preexisting foliation (Fig. 4b). This geometry must be distinguished from the S-C structures, which have been originally defined for a synkinematic pluton where S and C surfaces are formed synchronously (Berthé et al. 1979). During mylonitization, the granite experienced grain size reduction; undulatory quartz grains with lobate boundaries indicate dynamic recrystallization during low-temperature deformation (Fig. 4e). Recrystallization of such fine quartz grains may be due to combined subgrain rotation and bulging recrystallizations (Stipp et al., 2002). The asymmetry of feldspar porphyroclasts with sigma-type recrystallization tails (Fig. 4f), sigmoidal micafish (Fig. 4g), quartz ribbons, and shear band geometry suggest a non-coaxial strain regime with a top-to-the-NE sense of shear (Fig. 4h, Passchier and Trouw 2005), in agreement with a normal-dextral sense of the shear.

In deformed granite samples (AU02, AU03, AU04, AU20, SE01 and SE02, Fig. 6), quartz c-axis measurements reveal an incomplete type I crossed griddle pattern (Lister and

Hobbs 1980). Maxima around the main shortening direction axis (Z) indicate activity of basal <a> slip systems, and the dominant recrystallization mechanism is bulging recrystallization (Stipp et al. 2002). Submaxima distributed either close to the Y axis, or in between the Y and Z axes stem from prism <a> and rhomb <a> slips (Bouchez 1977), with dominant subgrain rotation recrystallization (Stipp et al. 2002). The coexistence of these slip systems may be due to different activation temperature; at ca. 300°C, basal <a> slip is dominant, whereas, at 500°C, prism <a> is more important (Bouchez 1977; Stipp et al. 2002; Passchier and Trouw 2005) However, at low temperature, with an increasing strain, the slip sequence is basal <a>, followed by prism <a>, and finally rhomb <a> (Passchier and Trouw 2005). Since basal <a> slips are mainly observed in protomylonites, and both prism <a> and rhomb >a> slips are dominant in the most deformed mylonites (Fig. 6), the second alternative seems more likely. The asymmetry of the c-axis maxima suggests a non-coaxial progressive deformation, under low to intermediate temperature, with a top-to-NE sense of shear in agreement with other kinematic indicators.

4. New geochronological data

To constrain the age of the granitoid emplacement and the time of the ductile deformation, monazite U-Th-Pb geochronology and micas $^{40}Ar/^{39}Ar$ dating have been carried out.

4.1. Electron microprobe (EPMA) monazite geochronology

The EPMA U-Th-Pb dating on monazite is a chemical method based on two main assumptions related to the mineral structure. (1) The common lead incorporated in monazite during crystallization is negligible compared to the amount of radiogenic lead (Parrish 1990; Cocherie et al. 1998), and (2) no radiogenic lead loss occurred since the system closure (considered as the crystallization time in magmatic rocks). These assumptions have been confirmed both by experimental studies, and by comparison of EPMA dating and conventional U/Pb isotopic methods (Cocherie et al. 1998; 2005; Montel et al. 2002). Moreover, altered domains with potential lead loss can be avoided with the EPMA resolution (2 μm) associated with Backscattered Electron (BSE) microscopy. This monazite EPMA method is well suited for the dating of leucogranite, as monazite is common in peraluminous granite (e.g. Bé Mézème et al. 2006).

In-situ monazite grains were analyzed with a Cameca SX 50 electron microprobe, co-operated by ITSO and BRGM, following the analytical procedure described in Cocherie et al. (1998). Acceleration voltage is 20 kV, beam current is 200 nA, and U, Th, Pb absolute errors are 105 ppm, 130 ppm and 110 ppm, respectively. The U-Th-Pb age calculations were done by using the "EPMA dating" program written by Pommier et al. (2002). The age calculated for each microprobe point analysis is rejected if out of the confidence range. The sorted results are computed and plotted with the ISOPLOT program (Ludwig 1999; 2003). Due to a relatively large range in Th/U ratios, the isochron method of Cocherie and Albarede (2001) was used to produce the U/Pb vs Th/Pb diagrams reported in Figure 6. The following parameters were extracted from the diagram and used to compute the best fit line age calculation for each sample: (1) Th-Pb age (intercept with Th/Pb axis) and U-Pb age (intercept with U/Pb axis) and their respective errors (2σ); (2) slope and error of the best fit line, X-Y coordinates of the centroid of the best fit line. The results are statistically acceptable if the following three conditions are fullfilled. : (1) The theoretical Mean Square Weight Deviation (MSWD) is above the calculated MSWD, (2) the theoretical isochron crosscuts the envelope error of each analysis and (3) the intercept ages are similar within the error margin.

In the studied samples, monazite grains are included in biotite and predate the crystallization of the mica (Fig 7a). BSE images (Fig. 7b) of monazite in the Autun undeformed leucogranite (AU16, N46°55’55’’; E4°19’22’’) show medium-sized euhedral to sub-euhedral grains (50 to 100 μm) with no significant chemical zoning. The data scatter is relatively good and an isochron age of 318±7 Ma has been calculated on 8 grains (Fig. 7b). The MSWD is slightly higher than the theoretical value (1.5 *vs.* 1.4).

BSE images of monazite in mylonitic Autun leucogranites sample (AU26, N46°57'00"; 4°21'35") show euhedral grains not deformed during the ductile event and still exhibiting typical growth zoning (Fig. 7c). Most of the analyses are clustered but, since some analyses show a high U/Pb ratio, a best fit line can be drawn, and an isochron age of 321±3 Ma has been calculated on 5 grains (Fig. 7c). The intercept ages (U-Pb age 323±6 Ma and Th-Pb age: 306±36 Ma) are similar within errors. The MSWD is largely below the theorical value (0.23 *vs.* 1.30), a statistically meaningful result.

BSE images of monazite in the La Serre granite (SE03, N47°10'20"; E5°33'24") show medium-sized sub-euhedral to anhedral grains (Fig. 7d). The data are widely spread in the isochron diagram and a best fit line can be drawn. The calculation on 6 grains provides an isochron age of 317±5 Ma (Fig. 7d). Although the theoretical isochron is at the limit of the error envelope of the best fit line, the results are acceptable as the intercept ages (U-Pb age 290±30 Ma and Th-Pb age: 338±25 Ma) are similar within error magin, and the calculated MSWD is slightly lower than its theoretical value (1.3 *vs.* 1.38).

4.2. Deformation and cooling age of the Autun and the La Serre granites

In order to date the ductile faulting and to constrain the relationships between magmatism and deformation, we performed $^{40}Ar/^{39}Ar$ dating on mylonites from the two shear zones and on the Autun granite, and assumed that muscovite and biotite ages from these samples would provide constraints on their cooling history in the 300°C-450°C range (Harrison et al. 1985, 2009; Hames and Bowring 1994). As these cooling temperatures are similar to those deduced from LPO measurements in mylonitic rocks, the $^{40}Ar/^{39}Ar$ method should give a reliable estimate of the age of deformation and an estimate of the cooling rate of the granite.

Details about the analytical procedure for laser probe $^{40}Ar/^{39}Ar$ dating can be found in York et al. (1981), Dalrymple (1989), McDougall and Harrison (1999), Monié et al. (1994) and Monié and Agard (2009). Each sample was first crushed and micas were separated under a binocular from the 0.5-07 mm size fraction. After ultrasonic cleaning, micas were enveloped in aluminium foils and irradiated at McMaster (Canada) together with several aliquots of the MMhb1 monitor amphibole (520.4 ± 1.7 Ma; Samson and Alexander 1987). After irradiation, the micas and standards were placed on a copper holder inside the sample chamber and heated at 150°C under ultrahigh vacuum. Step-heating degassing of individual grains was performed using a continuous CO_2 laser until complete fusion of the mineral. For each step, the released gas was cleaned on getters and then introduced in a MAP 215-250 mass spectrometer for analysis of the isotopic composition, estimated by regression on 15 runs. Extraction, cleaning, and analysing processes involve 1, 2 and 8 minutes respectively. System blanks were realized every three experiments. Depending on the samples, 9 to 17 steps were performed. Individual age (Tab. 1) was calculated after usual isotope corrections including blanks, mass discrimination, radioactive decay of ^{37}Ar and ^{39}Ar, and irradiation-induced mass interference. For the MAP 215-250 mass spectrometer, a $^{40}Ar/^{36}Ar$ ratio of 285.0 ± 2.0 was used for mass discrimination of all analyses. The uncertainty on the J-factor was propagated in the calculation of the error on the total age of each sample, equivalent to a K–Ar age. Results are reported as classical $^{40}Ar/^{39}Ar$ age spectra (Fig. 8).

The term "plateau age" is defined as the segment of a spectrum, made of three consecutive steps, containing more than 70% of the total ^{39}Ar released, and whose ages overlap within two sigma errors (McDougall and Harrison, 1999). Ages are reported with a 1σ uncertainty. It is worth to mention that the Autun shear zone experienced an important fluid circulation that caused silicification, galena mineralization and secondary large muscovite flake crystallization, probably during late brittle faulting (Delfour et al., 1991). Since this alteration event possibly influenced the argon isotopic system, only unaltered samples were choosen.

Biotite from the inner part of the Autun granitic massif shows a discordant spectrum with ages varying from 297 Ma to 308 Ma and a plateau age of 306.4 ± 4 Ma calculated on the last 70 % of ^{39}Ar released (sample AU29, N46°54'30"; E4°16'20", Fig. 8a). Muscovite from the Autun protomylonite (sample AU17, N46°56’9”; E4°19’10”, Fig. 8b) displays a slightly discordant spectrum with ages ranging from 261 to 355 Ma. More than 80 % of the total ^{39}Ar released gives a plateau age of 303.9 ± 3 Ma in the intermediate portion of the spectrum.

Biotite from the Autun granite (AU16, N46°55’55’’; E4°19’22’’, Fig. 8c) has a discordant spectrum with evidence of argon loss at the beginning of degassing and excess argon at the end, resulting in ages varying from 133 Ma to 310 Ma. A plateau age of 299.6 ± 3 Ma has been calculated on more than 75 % of ^{39}Ar released in the intermediate portion of the spectrum. Muscovite from sample AU16 (Fig. 8d) shows a relatively flat spectrum with values ranging mainly between 291 Ma and 301 Ma, with the exception of the first step related to argon bound to the mica surface. A plateau age of 299.8 ± 3 Ma is calculated for more than 80 % of the total ^{39}Ar released.

Biotite from the Autun mylonite (AU15, N46°56’24’’; E4°18’53’’, Fig. 8e) displays a highly discordant spectrum with ages varying from 220 Ma to 303 Ma and no plateau age. It is likely that incipient chloritization is responsible for such a pattern, with combined effects of argon loss and neutron-induced ^{39}Ar recoil (Turner and Cadogan, 1974; Ruffet et al., 1991). Muscovite from sample AU15 gives a much less discordant spectrum with young ages for low experimental temperatures (Fig. 8e). With the exception of the three first steps, the ages are bracketed between 295 and 304 Ma, and a plateau age of 299.8 ± 3.0 can be calculated on 95% of the total ^{39}Ar released.

Muscovite from the La Serre mylonite (sample SE01Ms, 47°11'19"; 5°31'27", Fig. 8f) displays a discordant spectrum ranging from 289 to 321 Ma, with argon excess released at low experimental temperature. However for 75 % of the total ^{39}Ar released, ages are bracketed between 296 Ma and 299 Ma and correspond to a plateau age of 298.2 ± 3 Ma. In this sample, the deformation is very strong, and biotite is often replaced by chlorite.

5. Discussion

5.1. Regional correlations of the Autun and La Serre Faults

The western and eastern continuations of Variscan shear zones in the northern French Massif Central remained speculative for a long time (Arthaud and Matte 1977). Rolin and Stussi (1991) considered the Autun Shear Zone as an Upper Devonian to Middle Carboniferous dextral wrench fault and, after restoring the sinistral offset of the Sillon Houiller Fault, correlated it with the Marche-Combrailles Fault (see also Lerouge and Quenardel 1985; Rolin & Colchen 2001). However, our new data and other recent ^{40}Ar-^{39}Ar dating in the La Marche area (Gebelin et al. 2007) indicate that the Marche-Combrailles and the Autun shear zones are two different shear zones. Recent geophysical studies also suggest that the eastern continuation of the Marche-Combrailles Fault is the Avallon Fault (Edel 2008; Fig. 9). The eastern continuation of the Autun Shear zone is less hypothetic, as shown by the similar structures observed along the La Serre Fault Zone. After restoring the E-W offset related to the Cenozoic opening of the Bresse graben, the two areas belong to the same fault system. However, vertical derivation of the Bouguer gravity anomaly map does not support a direct continuity between the two shear zones (Edel, unpublished data), but rather suggest that the Autun Shear Zone joins a fault zone parallel to the La Serre Shear Zone, located about 10 km to the north of the La Serre Shear Zone. The southwestern extension of the N65°E trending La Serre brittle Fault might be the fault that rims the Creusot Basin (Fig. 1). Presently, there is no evidence of the western continuation of the La Serre ductile shear zone to the Morvan area. The La Serre ductile shear zone may extend westward below the Creusot sedimentary basin. All these E-W to N65°E trending faults are crosscut by the La Serre Southern brittle Fault (Fig. 3), a segment of the NE-SW striking Sainte-Marie-Aux-Mines Fault. This sinistral fault hides the eastern extension of the Autun-La Serre fault system (Fig. 9). However, recent work on the Upper Rhine graben (Edel et al. 2007; Ustaszewski and Schmid 2007) and along the Rhine-Bresse Transfer Zone (Madritsch et al. 2008) indicate the presence beneath the Mesozoic sedimentary cover of a large set of NE-SW to E-W pre-Mesozoic steeply dipping faults that might represent the eastern continuations of the Autun-La Serre fault system (Fig. 9). These Variscan faults were locally reactivated by the Late Eocene-Oligocene extension in the Upper Rhine graben (Edel et al. 2007) or by the Pliocene shortening during formation of the Jura fold-and-thrust belt (Giamboni et al. 2004). The gentle curvature of the Autun La Serre Fault System, from an E-W trend, to the west, to an ENE-WSW trend, to the east, could be related to local block rotations either due to Late Variscan adjustments as suggested by Edel and Schulmann (2007) or by Oligocene extension in the Bresse graben, or due to Pliocene tectonics of the Jura Mountains.

5.2. Timing of the extensional processes

Microstructural observations, and shape and lattice preferred orientation analyses indicate several types of deformation. As deduced from quartz <c> axis measurements and chessboard pattern, the Autun and La Serre plutons underwent a high-temperature deformation, the mechanisms of which remains controversial; it could be either be due to prism <c> slip (Mainprice et al. 1986) or grain growth and boundary migration (Gapais and Barbarin 1986) or α to β quartz transition (Kruhl 1996). Whatever the mechanism is, deformation likely occurred during granite emplacement. Furthermore, low- to intermediate temperature shearing in protomylonites, mylonites and ultramylonites indicates a strain gradient from the pluton margin, where a tectonic fabric dominates, to the pluton core, where sub-solidus preferred orientation is prominent. Such a strain gradient could be due to localized deformation either during magma crystallization or under solid-state conditions after granite emplacement.

Monazite U-Th/Pb dating yields consistent ages at ca. 320-318 Ma (Namurian) for the Autun and La Serre granites and the Autun mylonitic granite, indicating that the U-Th-Pb system was not reset during deformation (Figs. 7 and 10). A modification of the chemistry of the monazite can occur in amphibolite facies shear zones (Berger et al. 2006) but, in the present case, the lack of core-and-mantle zoned grains and the preservation of growth zoning suggest that monazite grains did not recrystallize during mylonitization. Moreover, since the dated monazites are included in biotite, they predate the crystallization of the micas. Crystallization of magmatic monazite in peraluminous systems occurs during granite emplacement (Braun et al. 1998; Förster 1998), at temperatures of about 900°C (Cherniak et al. 2004). Thus, the monazite U-Th/Pb ages mirror the crystallization age of the magma. The Namurian age assignment is significantly different from the Stephanian age previously proposed for the Autun granite (Rolin and Stussi 1991) and from the Devonian U-Pb (TIMS) age proposed for the La Serre granite (Morre-Biot and Storet 1967). The consistency between our new monazite U-Th/Pb ages and the petrographic and microstructural observations reveals that mylonite formed at the expense of the Autun granite. During the pluton emplacement, a poorly defined subsolidus fabric was acquired. However, the significance of this magmatic preferred orientation is not clear and might be due to magmatic processes in the magma chamber or to a combination of magma dynamics and regional tectonics (Brun and Pons 1981).

Whatever the deformation gradient obtained in the Autun and La Serre areas might be, the Late Carboniferous $^{40}Ar/^{39}Ar$ ages around 300 Ma show a regional consistency (Figs. 8 and 10a). One interpretation could be that a Late Carboniferous thermal event reset the argon isotopic system, a phenomenon recognized for the Late Visean evolution in the central part of the French Massif Central (Faure et al. 2002). Although a Stephanian to Permian volcanism is recorded in the northeastern part of the French Massif Central (Carpena et al. 1987; Chévremont et al. 1999), it seems to be too scattered and too small in volume to have caused such a large thermal overprint.

Protomylonites and undeformed granite exhibit $^{40}Ar/^{39}Ar$ spectra with plateau ages ranging from 305 to 300 Ma (Fig. 8), representing the time when the cooling path of the granite intersected the mica closure temperature. Due to their different closure temperatures, the concordance between muscovite and biotite $^{40}Ar/^{39}Ar$ ages indicates a fast cooling between 400°C and 300°C. The $^{40}Ar/^{39}Ar$ plateau age of undeformed rocks is statistically undistinguishable from those of mylonites (Figs. 8 and 10a). The range of closure temperature of the two micas is similar to the temperature interval in which quartz lattice slip was activated. The Stephanian age thus likely corresponds to the time of the low-temperature non-coaxial ductile deformation experienced by the Autun and La Serre plutons. The age of this ductile deformation is furthermore constrained by the Lower Autunian (303 Ma to 290 Ma) sedimentary deposits of the Autun basin (Fig. 10). The earliest activity along the Autun-La Serre shear zone remains unknown, as ^{40}Ar-^{39}Ar dating only provides the age of the youngest ductile motion. Deformation the Autun-La Serre Fault System might have started before 305 Ma. However, several lines of evidence suggest that these granites are not syntectonic plutons. High-temperature post-solidus shearing could not be demonstrated in the analyzed rocks and only magmatic sub-solidus textures are observed in undeformed granites. Moreover, the time gap of at least 15 myrs between granite emplacement and the last shear motion would imply a long-lived localized tectonic zone. As described in the geological outline section, such a time gap is not documented in the French Massif Central, where the Namurian - Westphalian NW-SE extension was followed by the Stephanian - Permian NE-SW extension (Faure and Becq-Giraudon 1993; Faure 1995). If a syntectonic granite had been emplaced in Namurian times, it would probably have recorded the NW-SE stretching associated with the widespread first extensional stage, (Faure 1995; Talbot et al. 2005; Joly et al. 2009).

Our results demonstrate the existence of a Stephanian - Autunian NE-SW Autun-La Serre transtensional shear zone system. Its age is slightly younger than the Westphalian to Stephanian Pilat detachement fault that shows similar mechanisms and structures (Malavieille et al. 1990). Although well documented (Burg et al. 1994; Faure 1995), the Stephanian - Permian NE-SW stretching must be distinguished from the NW-SE Namurian - Westphalian extension reported from the western part of the Massif Central (Faure, 1995). Extensional structures are also documented beyond the Rhine Bresse transfer zone in the Vosges Mountains and Black Forest. Similar to the French Massif Central, the convergence of Gondwana and Laurussia has resulted in thrust tectonics and metamorphism in the Vosges Mountains (Fluck et al., 1987; Rey et al. 1989; Schulmann et al. 2002), and in the Black Forest (Wickert and Eisbacher, 1988; Eisbacher et al., 1989; Echtler and Chauvet 1992;). The thickened crust experienced syn-orogenic to post-orogenic extension represented by detachment faults and syntectonic plutons, documented in the Vosges Mountains (Rey et al. 1992; Kratinova et al. 2007), and in the Black Forest (Krohe and Eisbacher 1988; Eisbacher et al. 1989; Echtler and Chauvet, 1992).

5.3. Implications for the thermal conditions during post-orogenic extension

As ^{40}Ar-^{39}Ar ages of undeformed and deformed granites exhibit similar plateau ages around 300 Ma and are ca. 15 myrs younger than the monazite U-Th-Pb ages of pluton emplacement, the contemporaneity between the emplacement of plutons and the oblique-slip displacement along the Autun-La Serre Shear Zone is ruled out. However, additional geochronological studies are required to solve the question of « the synkinematic granites ».

Furthermore, the time gap of 15 myrs between U-Th/Pb ages and ^{40}Ar-^{39}Ar ages of the granite is larger than ca. 5 myrs cooling times from 750°C (emplacement temperature) to 300°C, experimentally established for similarly-sized leucogranites (Annen et al. 2006; Annen and Scaillet 2006). We propose two different cooling paths (Fig. 10b). One two-stage cooling path is characterized by a “normal cooling” during the first 5 myrs, with a 100°C/Myr cooling rate, followed by a 10 myrs steady-state step around 300°C; in this case, ^{40}Ar-^{39}Ar ages of micas in undeformed granites should be close to U-Th/Pb ages and significantly older than age of mylonitization. An alternative cooling model could be a single step path, with continuous cooling from 800°C at 320 Ma to 300°C at 305 Ma. Such a 500°C temperature drop in 15 myrs represents a 33°C/myr cooling rate. Such a slow rate would require a constant heat flow during the Late Carboniferous in order to maintain a high mean crustal temperature. The formation of the Velay migmatitic dome (Ledru et al. 2001) is characterized by a Late Carboniferous continuous melting of the metasediments of the lower crust. Crustal melting, assisted by underplating of mantle-derived magma (Williamson et al. 1996) from asthenospheric upwelling (Ledru et al. 2001), supports the existence of a regional high heat flow hypothesis in the Eastern Massif Central. However, this thermal anomaly remains limited to the Velay area, and indications of an important Westphalian and Stephanian magmatism are lacking in the Morvan, Vosges and Black Forest areas. The rare Stephanian shoshonites in the Epinac basin (Chévremont et al., 1999) cannot account for a continuous heat flow during the 315-300 Ma period. The most significant magmatic event recorded in

Morvan, Vosges and Black Forest areas dates back to Early Permian times (Lippolt and Hess, 1983; Carpena et al., 1987). The current available data do not allow to determine which cooling path did the Autun and La Serre plutons follow.

Whatever its path is, cooling was followed by ductile and brittle faulting along the Autun-La Serre transtensional fault system. The normal component deduced from field observations and microstructural analysis could have accommodated the rapid exhumation indicated by the cooling between 400°C and 300°C and by the rapid transition from ductile conditions along the shear zone at 300 Ma to brittle, normal, syn-sedimentary faulting at around 297 Ma (Figs. 8 and 10a). Such a ductile-brittle continuum is known in the Aegean extensional realm (Mehl et al. 2005) and also in the Massif Armoricain (Turrillot et al. submitted). In the Autun region, the ductile-brittle transition is also marked by a rotation of the stretching direction from NE-SW in Stephanian - Early Autunian times to N-S in Late Autunian times (Marteau 1983; Faure 1995). Under brittle conditions, exhumation continued during Autunian times, accomodated by normal faulting. Evidence for Autunian normal faulting can be observed in the sedimentary basin of Autun, where at least 1200 m of detrital lacustrine and fluviatile sediments accumulated (Chévremont et al. 1999). Moreover, in the sedimentary filling of the Autun basin, plant fragments were buried and transformed into coal. Coalification requires rapid burial to ensure the preservation of the organic matter. The huge abundance of coal in the Autun basin suggests that the subsidence of the basin was tectonically controlled and was probably coeval with a rapid exhumation of the Variscan basement.

In the northeastern French Massif Central, the post-orogenic evolution is characterized by Namurian - Westphalian granite emplacement followed by Stephanian - Autunian NE-SW extension. This last stage contributed to the exhumation of the Variscan rocks, although it remains difficult to propose an exhumation rate for the Stephanian - Permian period since the geothermal gradient at that time is unknown and since the estimation of the P-T conditions of the granite before the initiation of the deformation is not available. The two-stages extension interpretation agrees with Faure (1995) who pointed out that the Namurian - Westphalian extension is more pronounced in the western part of the French Massif Central than in the eastern part, where Stephanian to Permian extension is well recorded. The extensional processes thus appear to be subdivided into small intervals of regionally localized shearina and related to a large period of crustal melting.

6. Conclusion

New structural and geochronological data on the Autun and La Serre areas constrain the Late Variscan evolution of the northeastern part of the French Massif Central. The similarity between the Autun and La Serre shear zones suggests the existence of an ENE-WSW trending fault system, which was probably reactivated under brittle conditions during the Cenozoic. The major results include: 1) the recognition of normal-dextral ductile shear zones and 2) documentation of a diachronism of ca. 15 myrs between the Namurian - Westphalian pluton emplacement and the Stephanian - Permian extensional tectonics and basin subsidence. The Stephanian - Autunian Autun and La Serre shear zones affected the Namurian plutons during their post-emplacement cooling, but these plutons are not synkinematic. This shows that the widespread idea of synkinematic plutonism as as a characteristic of late-orogenic to post-orogenic extension suffers exceptions. Several points remain unclear, such as the tectonic setting during the emplacement of the Autun pluton. More detailed studies, such as a study of the anisotropy of the magnetic susceptibility of the pluton, could improve our understanding of the Namurian - Westphalian extensional stage and its relationships with plutonism.

Acknowledgements

This work is a part of F. Choulet's master thesis dissertation. Field and analytical expenses have been funded by ISTO and Chrono-environnement. Alain Cocherie is acknowledged for his help during monazite U-Th-Pb calculations. The authors thank G. Eisbaher and J-B Edel, for constructive review.

References

Annen C, Scaillet B (2006) Thermal evolution of leucogranites in extensional faults: implications for Miocene denudation rates in the Himalaya. Special Publication 268, Geological Society, London pp 309-326

Annen C, Scaillet B,. Sparks RSJ (2006) Thermal Constraints on the Emplacement Rate of a Large Intrusive Complex: The Manaslu Leucogranite, Nepal Himalaya. J Petrol 47:71-95

Arthaud F, Matte P (1977) Late Paleozoic strike-slip faulting in southern Europe and northern Africa: Result of a right-lateral shear zone between the Appalachians and the Urals. GSA Bull 88:1305-1320, doi: 10.1130/0016-7606.

Bé Mézème E, Cocherie A, Faure M, Legendre O, Rossi P (2006) Electron microprobe monazite geochronology of magmatic events: Examples from Variscan migmatites and granitoids, Massif Central, France. Lithos 87:276-288

Berger A, Herwegh M, Gnos E (2006) Deformation of monazite in an amphibolite-facies shear zone. Geochem Cosmochim Acta 70:18 Supp. 1 A47

Bergeron J (1889) Etude géologique du Massif ancien situé au Sud du Plateau Central. Thèse Fac. Sci. Paris Ann Sci Géol, Masson, Paris

Berthé D, Choukroune P, Jegouzo P (1979) Orthogneiss, mylonite and non coaxial déformation of granites: the example of the South Armorican Shear Zone. J Struct Geol 1:31-34

Bouchez J-L (1977) Plastic deformation of quartzites at low temperature in an area of natural strain gradient. Tectonophysics 39:25-50

Braun I, Montel J-M, Nicollet C (1998) Electron microprobe dating of monazite from high-grade gneisses and pegmatites of the Kerala Khondalite Belt, southern India. Chem Geol 146:65–85

Brun J-P, Pons J (1981) Strain patterns of pluton emplacement en a crust undergoing non-coaxial deformation, Sierra Morena, Southern Spain. J Struct Geol 3:219-229

Burg J-P, Matte P (1978) A cross-section through the French Massif Central and the scope of its Variscan geodynamic evolution. Ztg Dtsch Geol Ges 109:429-460

Burg J-P, Van den Driessche J, Brun J-P (1994) Syn-to post-thickening extension in the Variscan Belt of Western Europe: Modes and structural consequences. Géologie de la France 3:33-51.

Campy M, Chauve P, Pernin C (1983) Notice explicative de la carte géologique de Pesmes au 1:50000, Bureau de recherches géologiques et minières, Orléans

Carpena J, Doubinger J, Guérin R, Juteau J, Monnier M (1987) Le volcanisme acide de l'Ouest Morvan dans son cadre géologique: caractérisation géochimique, structurale et chronologique de mise en place. Bull Soc Géol Fr 7:839-859

Cherniak DJ, Watson EB, Grove M, Harrison TM (2004) Pb diffusion in monazite: a combine RBS/SIMS study. Geochem Cosmochim Acta 68:829-840

Chévremont P, Rémond C, Marteau P et al (1999) Notice explicative de la carte géologique d' Epinac-Les-Mines au 1:50000, Bureau de recherches géologiques et minières, Orléans

Cocherie A, Albarède F (2001) An improved U-Th-Pb age calculation for electron microprobe dating of monazite. Geochem Cosmochim Acta 65:4509-4522

Cocherie A, Legendre O, Peucat J-J, Kouamelan AN (1998) Geochronology of polygenetic monazites constrained by in situ electron microprobe Th-U-total Pb determination: implications for lead behaviour in monazite. Geochem Cosmochim Acta 62:2475-2497

Cocherie A, Bé Mézème E, Legendre O, Fanning CM, Faure M, Rossi P (2005) Electron-microprobe dating as a tool for determining the closure of Th-U-Pb systems in migmatitic monazites. Am Mineral 90:607-618

Coromina G, Fabbri O (2004) Late Palaeozoic NE-SW ductile-brittle extension in the La Serre horst, eastern France. C R Geoscience 336:75-84

Courel L (2001) Histoire tardi-hercynienne et couverture méso-cénozoïque. Géologues 130-131:47-49

Dalrymple GB (1989) The GLM continuous laser system for. ^{40}Ar/^{39}Ar dating: description and performance characteristics. US Geol Surv Bull 1890:89–96

Delfour J, Arène J, Clozier L, Carroue J-P, Cornet J, Delance J-H, Feys R, Lemière B (1991) Notice explicative de la carte géologique d'Autun au 1:50000, Bureau de recherches géologiques et minières, Orléans

Delfour J (1989) Données lithostratigraphiques et géochimiques sur le Dévono-Dinantien de la partie sud du faisceau du Morvan (nord-est du Massif Central français). Géologie de la France 4:49-77

Dewey J (1988) Extensionnal collapse of orogens. Tectonics 7:1123-1139

Duthou J-L, Cantagrel J-M, Didier J, Vialette Y (1984) Palaeozoic granitoids from the French Massif Central: age and origin studied by ^{87}Rb-^{87}Sr system. Phy Earth Planet Inter 35:131-144

Echtler H, Chauvet A (1992) Carboniferous convergence and subsequent crustal extension in the southern Schwarzwald (SW Germany). Geodin Acta 5:37-49

Echtler H, Malavieille J (1990) Extensional tectonics, basement uplift and Stephano-Permian collapse basin in a late Variscan metamorphic core complex (Montagne Noire, Southern Massif Central). Tectonophysics 177:125-138

Edel J-B, Schulmann K, Rotstein Y (2007) The Variscan tectonic inheritance of the Upper Rhine Graben: evidence of reactivations in the Lias, Late Eocene-Oligocene up to the recent. Int J Earth Sci 96:305-325

Edel J-B, Schulmann K (2007) Paleomagnetic constraints on the evolution of the Variscan belt in Carboniferous times. In: Schulmann K, Ledru P, Faure M, Lardeaux J-M (eds.) Mechanics of Variscan Orogeny: a modern view on orogenic research. Sept 2007, Orléans, Abstr Vol.

Edel J-B (2008) Structure et nature du socle anté-permien du Bassin de Paris d'après les données gravimétriques et magnétiques - Le problème de l'Anomalie Magnétique du Bassin de Paris (AMBP). Géochronique 105:31-37

Eisbacher GH, Lüschen E, Wickert F (1988) Crustal-scale thrusting and extension in the Hercynian Schwarzwald and Vosges, Central Europe. Tectonics 8:1-21

England PC, Thompson AB (1986) Some thermal and tectonic models for crustal melting in continental collision zones. In Coward MP, Ries AC (eds.) Collision tectonics. Geological society of London, Special Publication, 19:83-94

Faure M, Becq-Giraudon J-F (1993) Sur la succession des épisodes extensifs au cours du dés-épaississement carbonifère du Massif Central français. C R Acad Sci, Paris 316:967-973

Faure M, Pons J (1991) Crustal thinning recorded by the shape of the Namurian-Westphalian leucogranite in the Variscan Belt of the Northwest Massif Central, France. Geology 19:730-733

Faure M, Leloix C, Roig J-Y (1997) L'évolution polycyclique de la chaîne hercynienne. Bull Soc Géol Fr 168:839-859

Faure M, Bé Mézème E, Duguet M, Cartier C, Talbot J (2005) Paleozoic tectonic evolution of medio-europa from the example of the French massif central and massif armoricain. In: (eds.) Carosi R. Dias R. Iacopini D. and Rosenbaum G. The southern Variscan belt, Journal of the Virtual Explorer 19 (5)

Faure M, Bé Mézème E, Cocherie A, Rossi P, Chemenda A, Boutelier D (2008) Devonian geodynamic evolution of the Variscan Belt, insights from the French Massif Central and Massif Armoricain. Tectonics. doi:10.1029/2007TC002115.

Faure M, Monié M, Pin C., Malusky H, Leloix C (2002) Late Visean thermal event in the northern part of the French Massif central: new ^{40}Ar/^{39}Ar and Rb-Sr isotopic constraints on the Hercynian syn-orogenic extension. Int J Earth Sci (Geol Rundsch) 91:53-75

Faure M. (1995) Late orogenic carboniferous extensions in the Variscan French Massif Central. Tectonics 14:132-153.

Floc'h J-P (1983) La série métamorphique du Limousin central, Thèse, Univ. Limoges.

Fluck P, Edel J-B, Gagny C, Montigny R, Piqué A, Schneider J-L, Whitechurch H (1987) Le socle vosgien, segment de la chaîne varisque d'Europe : projet Vosges : état des connaissances, propositions d'axes de recherches. Géologie Profonde de la France, Docomuent BRGM 146

Förster HJ (1998) The chemical composition of REE-Y-Th-U-rich accessory minerals in peraluminous granites of the Erzgebirge-Fichtelgebirge region, Germany, Part I: The monazite (Ce)-brabantite solid solution series. Am Min 83:259-272

Franke W (1989) Variscan plate tectonics in Central Europe. Current ideas and open questions. Tectonophysics 169:221-228

Gapais D, Barbarin B (1986) Quartz fabric transition in a cooling syntectonic granite (Hermitage massif, France). Tectonophysics 125:357-370

Gébelin A, Brunel M, Monié P, Faure M, Arnaud N (2007) Transpressional tectonics and Carboniferous magmatism in the Limousin, Massif Central, France: Structural and $^{40}Ar/^{39}Ar$ investigations. Tectonics doi:10.1029/2005TC001822.

Giamboni M, Ustaszewski K, Schmid SM, Schumacher ME, Wetzel A (2004) Plio-Pleistocene Transpressional Reactivation of Paleozoic and Paleogene Structures in the Rhine-Bresse transform Zone (northern Switzerland and eastern France). Int J Earth Sci 93:207–223, doi. 10.1007/s00531-003-0375-2

Hames WE, Bowring SA (1994) An empirical evaluation of the argon diffusion in muscovite. Earth Planet Sci Lett 124:161-169.

Harrison TM, Duncan I, McDougall I (1985) Diffusion of ^{40}Ar in biotite : temperature, pessure and compositional effects. Geochim Cosmochim Acta 49:2461-2468

Harrison TM, Celerier J, Aikman AB, Hermann J, Heizler MT (2009) Diffusion of ^{40}Ar in muscovite, Geochim Cosmochim Acta 73:1039-1051.

Hibbard M.J. (1987) Deformation of incompletely crystallized magma systems: granitic gneisses and their tectonic implications. J Geol 95:543-561

Joly A, Faure M, Martelet G, Chen Y, (2009) Gravity inversion, AMS and geochronological investigations of syntectonic granitic plutons in the southern part of the Variscan French Massif Central. J Struct Geol 31:421-443

Kratinova Z, Schulmann K, Edel J-B, Ježek J, Schaltegger U (2007) Model of successive granite sheet emplacement in trantensionnal setting: Integrated microstructural and anisotropy of magnetic susceptibility study. Tectonics doi:10.1029/2006TC002035

Krohe A, Eisbacher GH (1988) Oblique crustal detachment in the Variscan Schwarzwald, southwestern Germany. Geol Rdsch 77:25-43

Kruhl JH (1996) Prism- and basal-plane parallel subgrain boundaries in quartz: a microstructural geothermobarometer. J Metam Geol 14:581-589

Lardeaux JM, Ledru P, Daniel I, Duchêne S (2001) The Variscan Drench Massif Central – a new addition to the ultra-high pressure metamorphic “club”: exhumation processes and geodynamic consequences. Tectonophysics 323:143-167

Launeau P, Robin P-YF (2005) Determination of fabric and strain ellipsoids from measured sectional ellipses – Implementation and applications. J Struct Geol 27:2223-2233

Ledru P, Lardeaux J-M, Santallier D, Autran A, Quenardel J-M, Floch J-P, Lerouge G, Maillet N, Marchand J, Ploquin A (1989) Où sont les nappes dans le Massif Central français? Bull Soc Géol Fr 8:605-618

Ledru P, Courrioux G, Dallain C, Lardeaux J-M, Montel J-M, Vanderhaeghe O, Vitel G (2001) The Velay dome (French Massif Central): melt generation and granite emplacement during orogenic evolution. Tectonophysics 342:207-237

Leloix C, Faure M, Feybesse J-L (1999) Hercynian polyphase tectonics in north-east French Massif Central: the closure of the Brévenne Devonian-Dinantian rift. Int J Earth Sci 88:409-421

Lerouge G, Quenardel J-M (1985) Chronologie des événements tectoniques dans le Nord-Ouest du Massif Central français et le Sud du bassin de Paris du Carbonifère inférieur au Plio-quaternaire. C R Acad Sci, Paris 301:621-626.

Lippolt HJ, Hess JC (1983) Isotopic evidence for the stratigraphic position of the Saar-Nahe Rotliegend volcanism, I 40Ar/40K and 40Ar/39Ar investigations. N Jb Geol Paläont 713-730.

Lister GS, Hobbs BE (1980) The simulation of fabric development during plastic deformation and its application to quartztite: the influence of deformation history. J Struct Geol 2:355-371

Ludwig KR (1999) Users manual for ISOPLOT/EX, version 2. A geochronological toolkit for Microsoft Excel – Berkeley Geochronology Center, Special Publication 1a

Ludwig KR (2003) User's manual for Isoplot 3.00. A geochronological toolkit for Microsoft Excel. Berkeley Geochronology Center, 70 p.

Madritsch H, Schmid SM, Fabbri O (2008) Interactions between thin- and thick-skinned tectonics at the northwestern front of the Jura fold-and-thrust belt (eastern France). Tectonics. doi:10.1029/2008TC002282.

Mainprice D, Bouchez J-L, Blumenfeld P, Tubia J-M (1986) Dominant c-slip in naturally deformed quartz: implications for dramatic plastic softening at high temperature. Geology 14:819-822

Malavielle J, Guilhot P, Costa S, Lardeaux J-M, Gardien V (1990) Collapse of the thickened Variscan crust in the French Massif Central: Mount Pilat extensional shear zone and St-Etienne upper Carboniferous basin. Tectonophysics 177:139-149

Malavieille J (1987) Kinematics of compressional and extensional ductile shearing deformation in a metamorphic core complex of the northeastern Basin and Range. J Struct Geol 9:541-554

Marteau P (1983) Le bassin permo-carbonifère d'Autun. Stratigraphie, sédimentologie et aspects structuraux. Document BRGM, 64

Mattauer M, Brunel M, Matte P (1988) Failles normales ductiles et grands chevauchements. Une nouvelle analogie entre l'Himalaya et la chaîne hercynienne du Massif central français. C R Acad Sci, Paris 306:671–676

Matte P (1986) Tectonics and plate tectonics model for the Variscan Belt of Europe. Tectonophysics 126:329-374

Matte P (2001) The Variscan collage and orogeny (480-290 Ma) and the tectonic definition of the Armorica microplate: a review. Terra Nova 13:117-121

Matte P (1991) Accretionary history and crustal evolution of the Variscan Belt in western Europe. Tectonophysics 196:309-337

McClay KR, Norton MG, Coney P, Davis GH (1986) Collapse of the Caledonian orogen and the Old Red Sandstones. Nature 323:147-149

McDougall I, Harrison TM (1999) Geochronology and Thermochronology by the ^{40}Ar/^{39}Ar method. Oxford University Press, New york, USA

Mehl C, Jolivet L, Lacombe O (2005) From ductile to brittle: evolution and localization of deformation below a crustal detachment (Tinos, Cyclades, Greece) Tectonics doi:4010.1029/2004TC001767

Ménard G, Molnar P (1989) Collapse of a Hercynian Tibetan Plateau into a late Palaeozoic European Basin and Range province. Nature 334:235-237

Monié P, Torres-Roldan RL, Garcia-Casco A (1994) Cooling and exhumation of the western Betic Cordilleras, 40Ar/39Ar thermochronological constraints on a collapsed terrane. Tectonophysics 238:353-379

Monié P, Agard P (2009) Coeval blueschist exhumation along thousands of km : implications for subduction channel processes, Geochem Geophys Geosyst 10, Q07002, doi:10.1029/2009GC002428.

Montel J-M, Devidal JL, Avignant D (2002) X-ray diffraction study of brabantite-monazite solid solutions. Chem Geol 191:89-104

Moore AC (1970) Descriptive terminology for the textures of rocks in granulite facies terrains. Lithos 3:123-127

Morre-Biot N, Storet J (1967) Sur l'age absolu du granite de la Serre. C R Acad Sci, Paris 265:1869-1870

Morre-Biot N (1969) Étude pétrologique du socle cristallin du massif de la Serre, Bull BRGM (2e série) I 3, 1-16.

Norton MG (1986) Late Caledonide extension in western Norway: a response to extreme crustal thickening. Tectonics 5:195-204

Ogg JG, Ogg G, Gradstein FM (2008) The Concise Geologic Time Scale. Cambridge University Press.

Parrish RR (1990) U-Pb dating of monazite and its application to geological problems. Can J Earth Sci 27:1431-1450

Passchier CW, Trouw RAJ (2005). Microtectonics. Springer

Pin C, Dupuy C, Peterlongo J-M (1982) Répartition des terres rares dans les roches volcaniques basiques dévono-dinantiennes du nord-est du Massif central. Bull Soc Géol Fr 7:669-676

Pin C, Peucat JJ (1986) Ages des episodes de métamorphisme paléozoïques dans le Massif central et le Massif armoricain. Bull Soc Géol Fr 8:461-469

Pin C (1990) Variscan oceans: ages, origins and geodynamic implications inferred from geochemical and radiometric data. Tectonophysics 177:215-227

Pommier A, Cocherie A, Legendre O (2002) EPMA Dating User's Manual: Age Calculation from Electron Probe Microanalyser Measurements of U–Th–Pb. BRGM Documents, 9 p.

Quenardel J-M, Rolin P (1984) Palaeozoic evolution of the Plateau d'Aigurande (NW Massif Central, France). Special Publications 14, Geological Society, London, pp 63-70

Rey P, Burg J-P, Lardeaux J-M, Fluck P (1989) Evolutions contrastées dans les Vosges orientales: témoins d'un charriage dans la chaine varisque. C R Acad Sci, Paris 309:815-821

Rey P, Burg J-P, Caron J-M (1992) Middle and Late Carboniferous extension in the Variscan belt: structural and petrological evidence from the Vosges massif (eastern France). Geodin Acta 5:17–36

Reynolds SJ, Spencer JE (1985) Evidence for large-scale transport on the Bullard detachment fault, west-central Arizona. Geology 13:353-356

Roig J-Y, Faure M (2000) La tectonique cisaillante polyphasée du S. Limousin (Massif central français) et son interprétation dans un modèle d'évolution polycyclique de la chaîne hercynienne. Bull Soc Géol Fr 171:295-307

Rolin P, Colchen M (2001) Carte structurale du socle Varisque Vendée-Seuil du Poitou-Limousin. Géologie de la France, 1-2:3-6

Rolin P, Stussi J-M (1991) Décrochements intracrustaux et intrusions granitiques carbonifères dans le Morvan (Massif central français). Bull Soc Géol Fr 162:839-859

Ruffet G, Féraud G, Amouric M (1991) Comparison of ^{40}Ar-^{39}Ar conventional and laser dating of biotites from the North Trégor Batholith. Geochim Cosmochim Acta 55:1675-1688.

Samson SD, Alexander ECJ (1987) Calibration of the interlaboratory ^{40}Ar–^{39}Ar dating standard, MMhb-1. Chem Geol 66:27–34

Schulmann K, Schaltegger U, Jezek J, Thompson A, Edel J-B (2002) Rapid burial and exhumation during orogeny: thickening and synconvergent exhumation of thermally weakened and thinned crust (Variscan orogen in western Europe). Am J Sci 302:856-879

Simpson C, Wintsch RP (1989) Evidence for deformation-induced K-feldspar replacement by myrmekite. J Metamorph Geol 7:261–275

Stipp M, Stünitz H, Heilbronner R, Schmid SM (2002) The eastern Tonale fault zone: a “natural laboratory” for crystal plastic deformation of quartz over a temperature range from 250 to 750 °C. J Struct Geol 24:1861-1884

Talbot J-Y, Martelet G, Courrioux G, Chen Y, Faure M (2004) Emplacement in an extensional setting of the Mont Lozère-Borne granitic complex (SE France) inferred from comprehensive AMS, structural and gravity studies. J Struct Geol 26:11-28

Talbot J-Y, Faure M, Chen Y, Martelet G (2005) Pull-Apart emplacement of the Margeride granitic complex (French Massif Central). Implications for the late evolution of the Variscan orogen. J Struct Geol 27:1610-1629

Turner G, Cadogan PH (1974) Possible effects of ^{39}Ar recoil in ^{40}Ar-^{39}Ar dating. Proceedings of the Fifth Lunar Science Conference 2:1601-1615

Ustaszewski K, Schmid SM (2007) Latest Pliocene to recent thick-skinned tectonics at the Upper Rhine Graben - Jura Mountains junction. Swiss Journal of Geosciences 100:293-312

Vallé B, Courel L, Gélard J-P (1988) Les marqueurs de la tectonique synsédimenatire et syndiagénétique dans le bassin stéphanien à régime cisaillant de Blanzy-Montceau (Massif Central, France). Bull Soc Géol Fr 8, IV 4:529-540

Wickert F, Eisbacher GH (1988) Two-sided Variscan thrust tectonics in the Vosges Mountains, northeastern France. Geodin Acta 2:101–120

Williamson BJ, Shaw A, Downes H, Thirlwall MF (1996) Geochemical constraints on the genesis of Hercynian two-mica leucogranites from the Massif Central, France. Chem Geol 127:25-42

York D, Hall CM, Yanase Y, Hanes JA, Kenyon WJ, (1981) ^{40}Ar/^{39}Ar dating of terrestrial minerals with a continuous laser. Geophys Res Lett 8:1136-1138.

Figure captions

Figure 1: Geological map of the NW French Massif Central and the Vosges (modified after Fluck et al., 1987; Coromina and Fabbri, 2004; Faure et al. 2008). Location of the Autun and La Serre areas are also represented. AU: Autun Basin; EP: Epinac Basin; LC: Le Creusot Basin; SH: Sillon Houiller; MCSZ: La Marche-Combrailles Shear Zone; ASZ: Autun Shear Zone; SMF: La Serre Median Fault ; SMMF: Sainte-Marie-aux-Mines Fault.

Figure 2: a): Simplifed geological map of the Autun area; b) cross section of the Autun area c) stereoplots of foliations and lineations observed in the granite and along the mylonitic zone.

Figure 3: a): Simplifed geological map of the la Serre area (modified after Coromina and Fabbri, 2004); b) cross section of the La Serre area c) stereoplots of foliations and lineations observed in the granite and in the mylonite.

Figure 4: Microstructure of the granite and the mylonite of the Autun and La Serre shear zones. Bt: biotite; Ms: muscovite; Ort: orthoclase; Plg: plagioclase; Qz: quartz. a: undeformed, with weak preferred orientation Autun leucogranite, b: Shear bands (yellow) cutting primary magmatic foliation (red) in Autun mylonite, c: chessboard texture in quartz showing prismatic subgrains in the La Serre granite, d: myrmekite indicating syn-magmatic deformation of the Autun granite, e: dynamically recrystallized quartz ribbons in the La Serre mylonite, f: mantle porphyroclasts of a K-feldspar in Autun mylonite, with a σ-type shear criterion, g: muscovite micafish in shear bands in Autun mylonite, h: detail of elongated newly formed quartz grains developed by dynamic recrystallization in Autun mylonite.

Figure 5: 3D fabric of Autun granites and mylonites deduced from preferred orientation of mica in three perpendicular planes. AU19 and AU16 are granites, AU20 and AU02 are mylonites. Manual (Man.) and automatic (Auto.) measurements of the orientation

of elongated micas are given in rose diagrams with 10° equal intervals (see text for more explanation).

Figure 6: Universal Stage measurements of the lattice preferred orientation of the quartz c-axes of Autun granite (a) and La Serre granite (b). Schmidt stereographic net (lower hemisphere) was used for projecting quartz c-axes. Contours are 1, 2, 3, 4, 5, 6, 7, 8% for 1% area. For each area, the mylonite shows a well-developed quartz c-axis maximum representative of crystal plasticity. The magmatic fabric in granite presents a high-temperature preferred orientation.

Figure 7: a: Photomicrograph of a monazite grain enclosed in biotite in the La Serre granite. Ap: Apatite; Bt: biotite; Mzt: monazite; Ort: orthoclase; Plg: plagioclase; Qz: quartz. b, c and d) : Isochron Th/Pb vs. U/Pb diagrams of samples AU16, AU26 SE03. For each rock, examples of Back-Scattered Electron Scan Electron Microscope images of analyzed monazite grains are shown. See sample locations in Fig. 2 and Fig. 3.

Figure 8: $^{40}Ar/^{39}Ar$ age spectra of Autun granite and mylonite (a to e)) and La Serre mylonites (f). See location in Fig. 2 and Fig. 3.

Figure 9: Simplified basement map of northeastern France. Deep Carboniferous basins and faults are modified after Ustaszewski et al. (2007) and hidden leucogranites are inferred from the gravimetric map of Edel (2008).

Figure 10: Synoptic chart of new geochronological data, showing that a ca. 15 myrs time gap separates the pluton emplacement and the ductile deformation. Two possible cooling paths of Autun and La Serre plutons are depicted.

Table 1 $^{40}Ar/^{39}Ar$ analytic data.

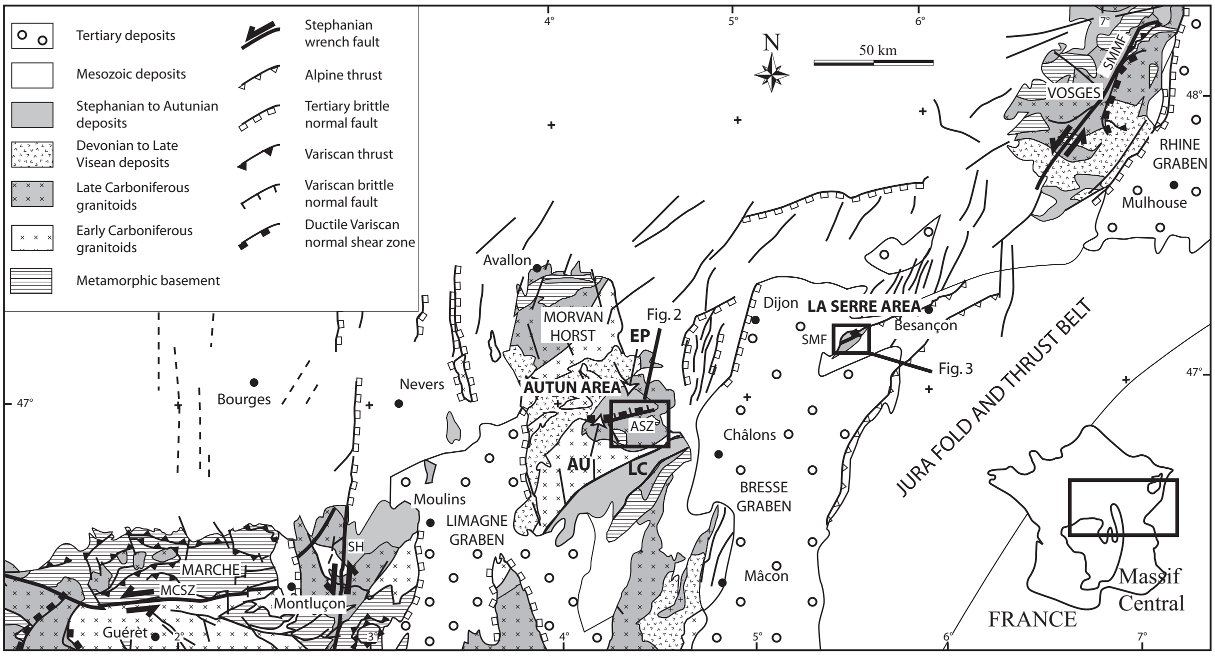
Tertiary deposits
Mesozoic deposits
Stephanian to Autunian deposits
Devonian to Late Visean deposits
Late Carboniferous granitoids
Early Carboniferous granitoids
Metamorphic basement
Stephanian wrench fault
Alpine thrust
Tertiary brittle normal fault
Variscan thrust
Variscan brittle normal fault
Ductile Variscan normal shear zone
N
50 km
VOSGES
SMMF
RHINE GRABEN
Mulhouse
Avallon
MORVAN HORST
Fig. 2
EP
Dijon
LA SERRE AREA
Besançon
SMF
Fig. 3
AUTUN AREA
ASZ
Nevers
Bourges
AU
LC
Châlons
BRESSE GRABEN
JURA FOLD AND THRUST BELT
Moulins
LIMAGNE GRABEN
SH
MARCHE
MCSZ
Montluçon
Guérèt
Mâcon
FRANCE
Massif Central
47°
48°
2°
3°
4°
5°
6°
7°

Figure 1

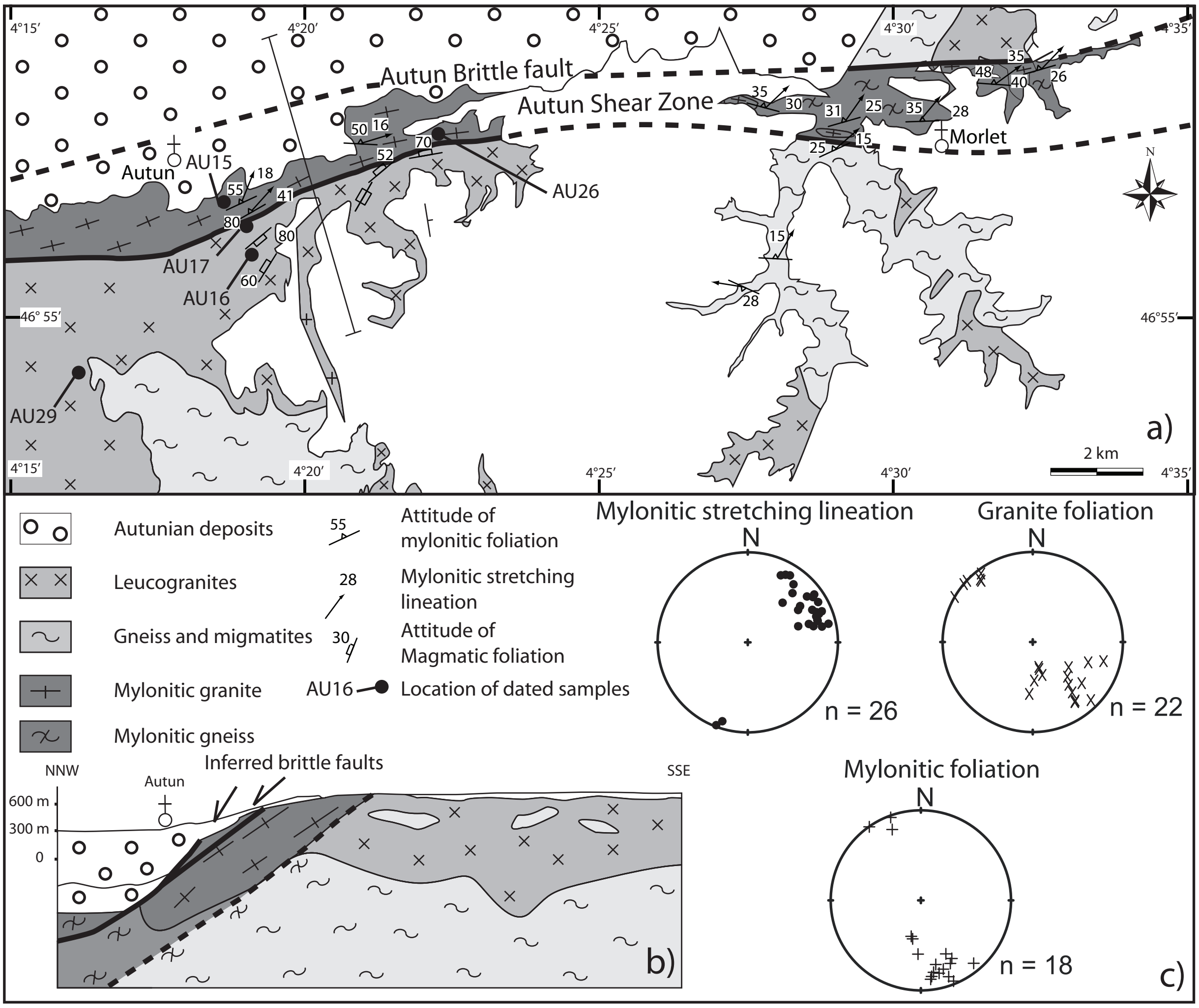
Autun Brittle fault
Autun Shear Zone
Autun
AU15
AU17
AU16
AU26
AU29
Morlet
a)
2 km
4°15′
4°20′
4°25′
4°30′
4°35′
46° 55′
46°55′
Autunian deposits
Leucogranites
Gneiss and migmatites
Mylonitic granite
Mylonitic gneiss
Attitude of mylonitic foliation
Mylonitic stretching lineation
Attitude of Magmatic foliation
Location of dated samples
NNW
SSE
Inferred brittle faults
600 m
300 m
0
b)
Mylonitic stretching lineation
N
n = 26
Granite foliation
N
n = 22
Mylonitic foliation
N
n = 18
c)

Figure 2

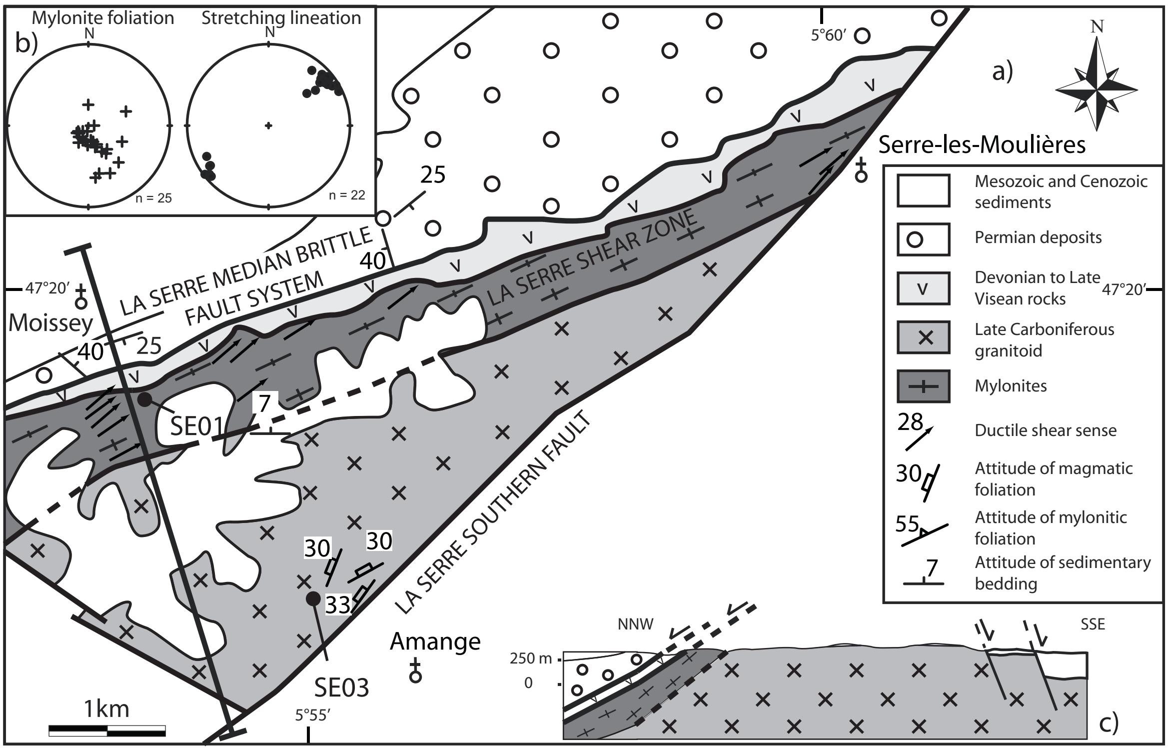
Mylonite foliation
Stretching lineation
b)
N
N
n = 25
n = 22
5°60′
a)
N
Serre-les-Moulières
25
LA SERRE MEDIAN BRITTLE
FAULT SYSTEM
LA SERRE SHEAR ZONE
40
47°20′
Moissey
40
25
SE01
7
30
30
33
LA SERRE SOUTHERN FAULT
Amange
SE03
1km
5°55′
Mesozoic and Cenozoic sediments
Permian deposits
Devonian to Late Visean rocks
47°20′
Late Carboniferous granitoid
Mylonites
28
Ductile shear sense
30
Attitude of magmatic foliation
55
Attitude of mylonitic foliation
7
Attitude of sedimentary bedding
NNW
SSE
250 m
0
c)

Figure 3

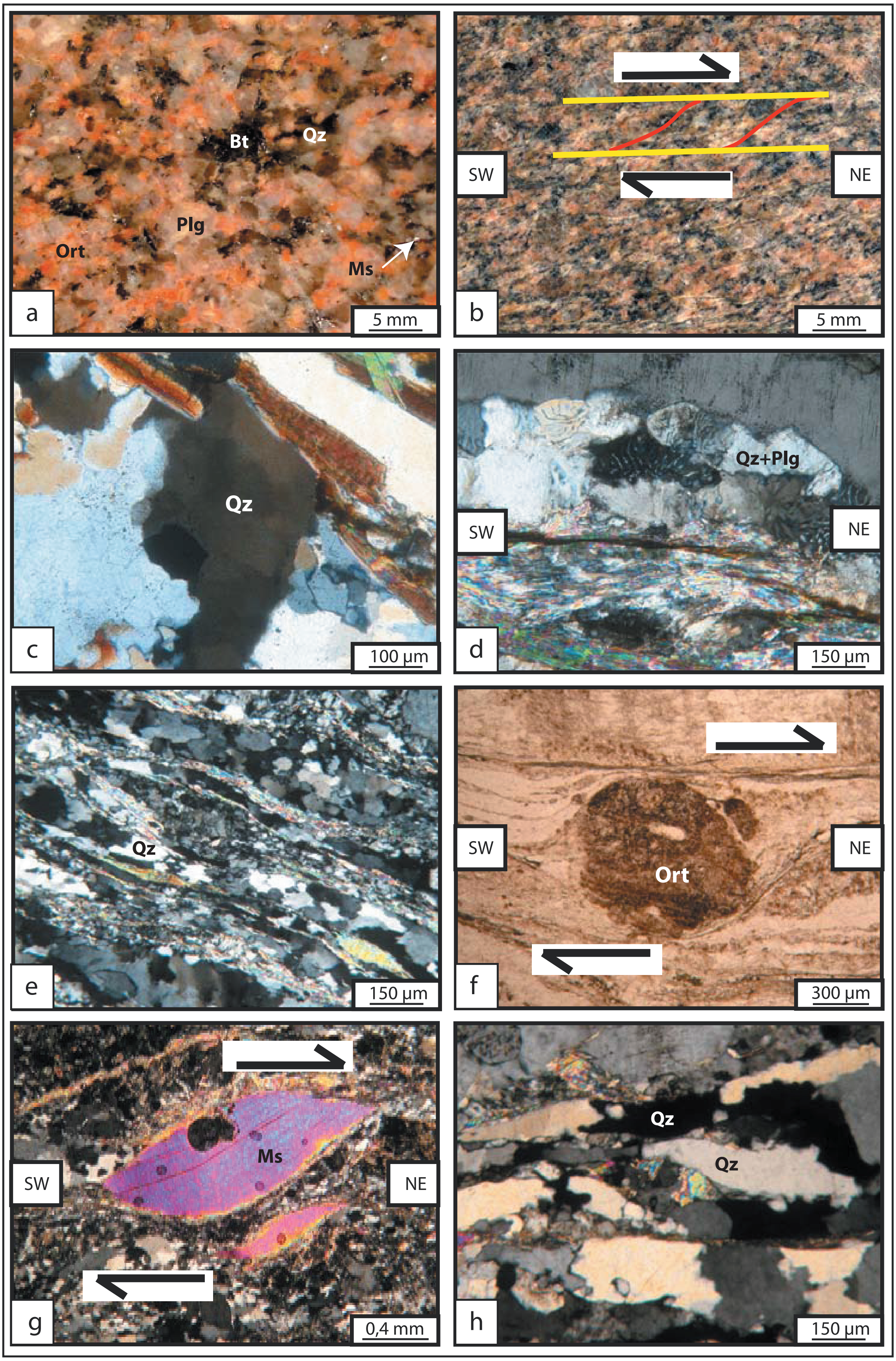
Bt
Qz
Plg
Ort
Ms
a
5 mm
SW
NE
b
5 mm
Qz
c
100 µm
Qz+Plg
SW
NE
d
150 µm
Qz
e
150 µm
SW
NE
Ort
f
300 µm
SW
NE
Ms
g
0,4 mm
Qz
Qz
h
150 µm

893

Figure 4

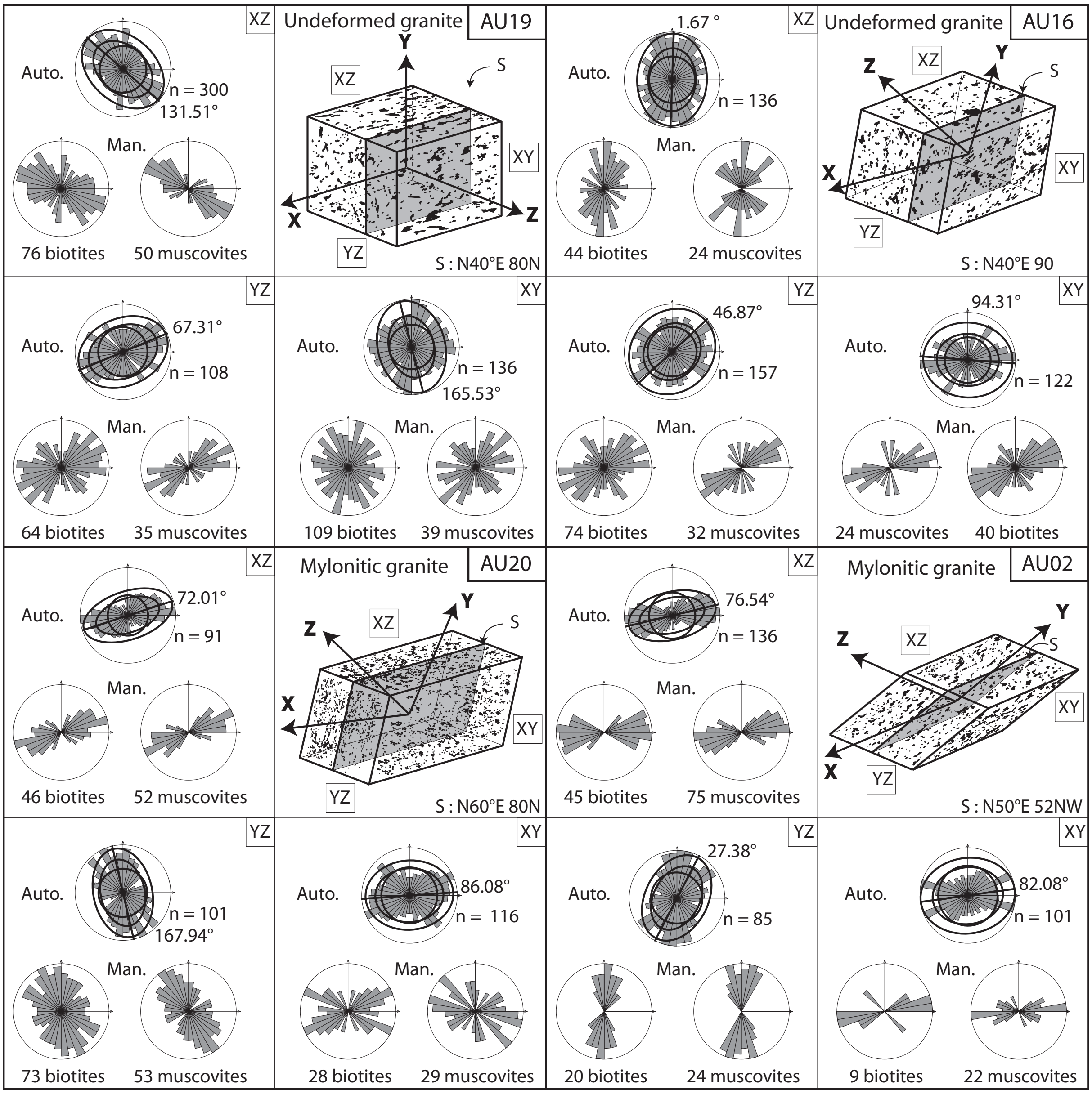
Undeformed granite
AU19
XZ
YZ
XY
Auto.
n = 300
131.51°
Man.
76 biotites
50 muscovites
S : N40°E 80N
Undeformed granite
AU16
1.67 °
n = 136
44 biotites
24 muscovites
S : N40°E 90
67.31°
n = 108
64 biotites
35 muscovites
n = 136
165.53°
109 biotites
39 muscovites
46.87°
n = 157
74 biotites
32 muscovites
94.31°
n = 122
24 muscovites
40 biotites
Mylonitic granite
AU20
72.01°
n = 91
46 biotites
52 muscovites
S : N60°E 80N
Mylonitic granite
AU02
76.54°
n = 136
45 biotites
75 muscovites
S : N50°E 52NW
n = 101
167.94°
73 biotites
53 muscovites
86.08°
n = 116
28 biotites
29 muscovites
27.38°
n = 85
20 biotites
24 muscovites
82.08°
n = 101
9 biotites
22 muscovites
X
Y
Z
S
Figure 5

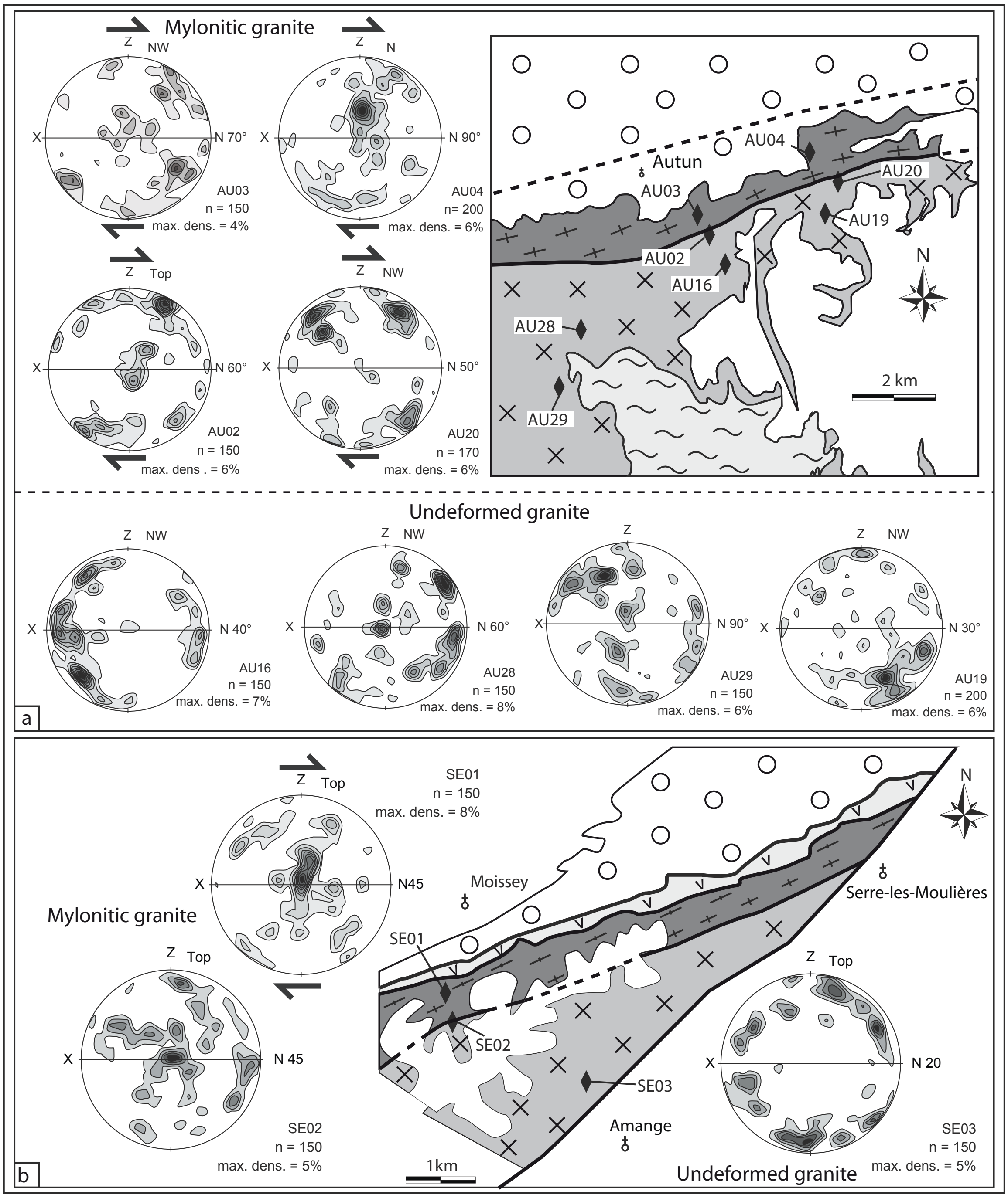

Mylonitic granite
Z NW
X
N 70°
AU03
n = 150
max. dens. = 4%
Z N
N 90°
AU04
n= 200
max. dens. = 6%
Z Top
N 60°
AU02
n = 150
max. dens . = 6%
Z NW
N 50°
AU20
n = 170
max. dens. = 6%
Autun
AU03
AU04
AU20
AU19
AU02
AU16
AU28
AU29
N
2 km
Undeformed granite
Z NW
N 40°
AU16
n = 150
max. dens. = 7%
Z NW
N 60°
AU28
n = 150
max. dens. = 8%
Z
N 90°
AU29
n = 150
max. dens. = 6%
Z NW
N 30°
AU19
n = 200
max. dens. = 6%
a
Z Top
SE01
n = 150
max. dens. = 8%
N45
Mylonitic granite
Moissey
Serre-les-Moulières
SE01
SE02
SE03
Amange
Z Top
N 45
SE02
n = 150
max. dens. = 5%
Z Top
N 20
SE03
n = 150
max. dens. = 5%
1km
Undeformed granite
b

Figure 6

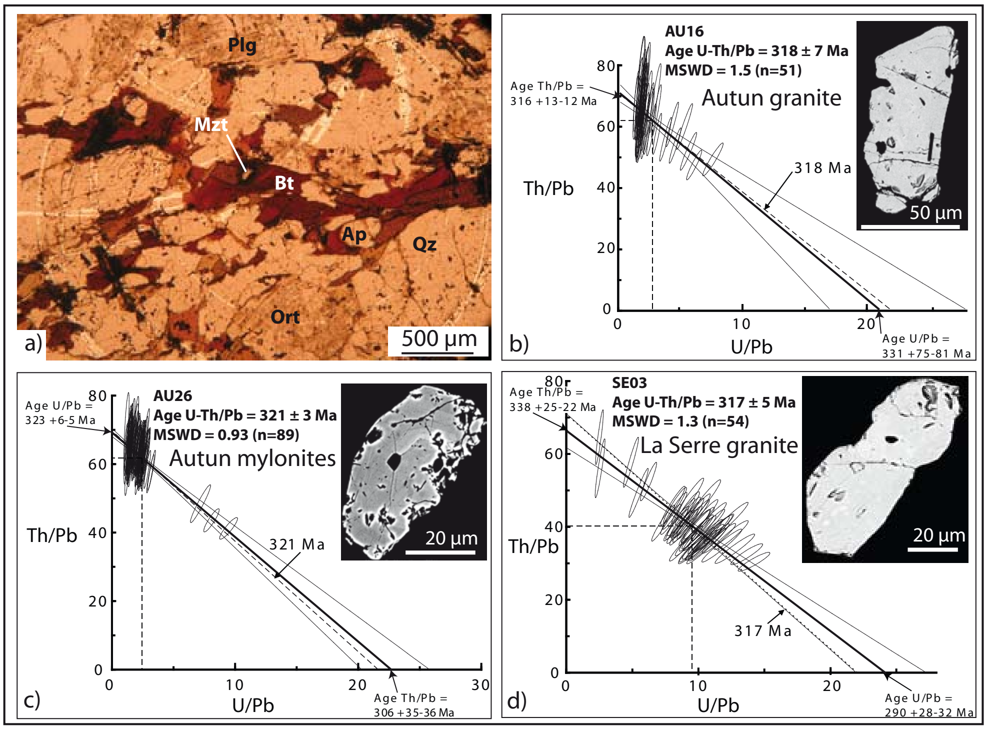
Plg
Mzt
Bt
Ap
Qz
Ort
500 µm
a)
AU16
Age U-Th/Pb = 318 ± 7 Ma
MSWD = 1.5 (n=51)
Autun granite
Age Th/Pb = 316 +13-12 Ma
318 Ma
50 µm
Th/Pb
U/Pb
Age U/Pb = 331 +75-81 Ma
b)
AU26
Age U-Th/Pb = 321 ± 3 Ma
MSWD = 0.93 (n=89)
Autun mylonites
Age U/Pb = 323 +6-5 Ma
321 Ma
20 µm
Th/Pb
U/Pb
Age Th/Pb = 306 +35-36 Ma
c)
SE03
Age U-Th/Pb = 317 ± 5 Ma
MSWD = 1.3 (n=54)
La Serre granite
Age Th/Pb = 338 +25-22 Ma
317 Ma
20 µm
Th/Pb
U/Pb
Age U/Pb = 290 +28-32 Ma
d)
Figure 7

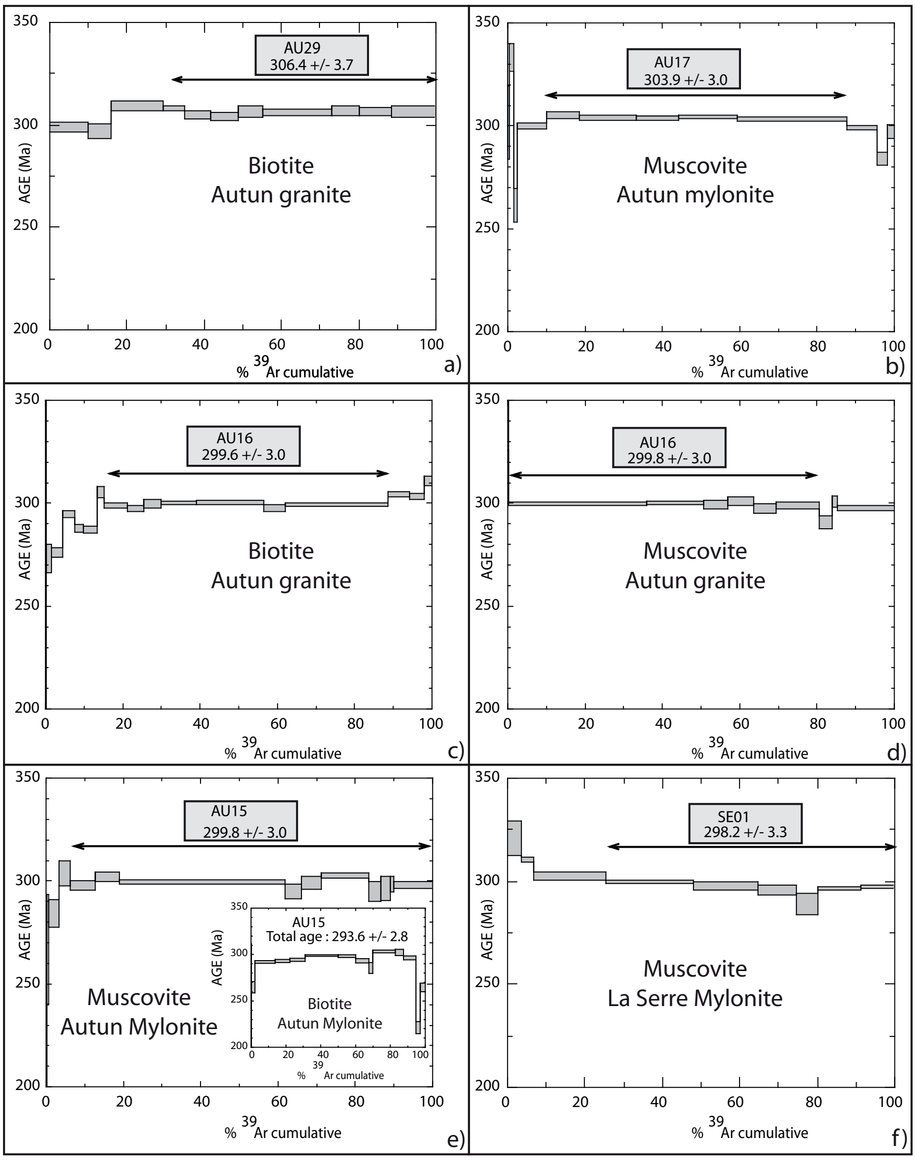

Figure 8

901

902

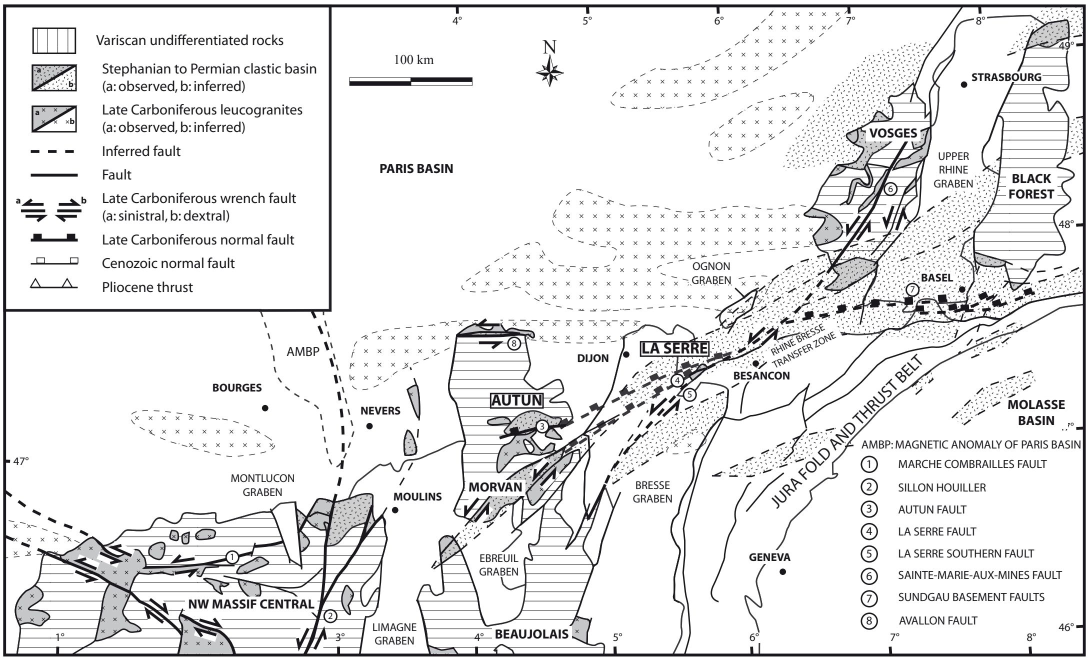
Variscan undifferentiated rocks
Stephanian to Permian clastic basin
(a: observed, b: inferred)
Late Carboniferous leucogranites
(a: observed, b: inferred)
Inferred fault
Fault
Late Carboniferous wrench fault
(a: sinistral, b: dextral)
Late Carboniferous normal fault
Cenozoic normal fault
Pliocene thrust
100 km
N
PARIS BASIN
AMBP
BOURGES
NEVERS
MONTLUCON GRABEN
MOULINS
NW MASSIF CENTRAL
LIMAGNE GRABEN
AUTUN
MORVAN
EBREUIL GRABEN
BEAUJOLAIS
DIJON
LA SERRE
OGNON GRABEN
BESANCON
RHINE BRESSE TRANSFER ZONE
BRESSE GRABEN
GENEVA
JURA FOLD AND THRUST BELT
VOSGES
STRASBOURG
UPPER RHINE GRABEN
BLACK FOREST
BASEL
MOLASSE BASIN
AMBP: MAGNETIC ANOMALY OF PARIS BASIN
1 MARCHE COMBRAILLES FAULT
2 SILLON HOUILLER
3 AUTUN FAULT
4 LA SERRE FAULT
5 LA SERRE SOUTHERN FAULT
6 SAINTE-MARIE-AUX-MINES FAULT
7 SUNDGAU BASEMENT FAULTS
8 AVALLON FAULT

Figure 9

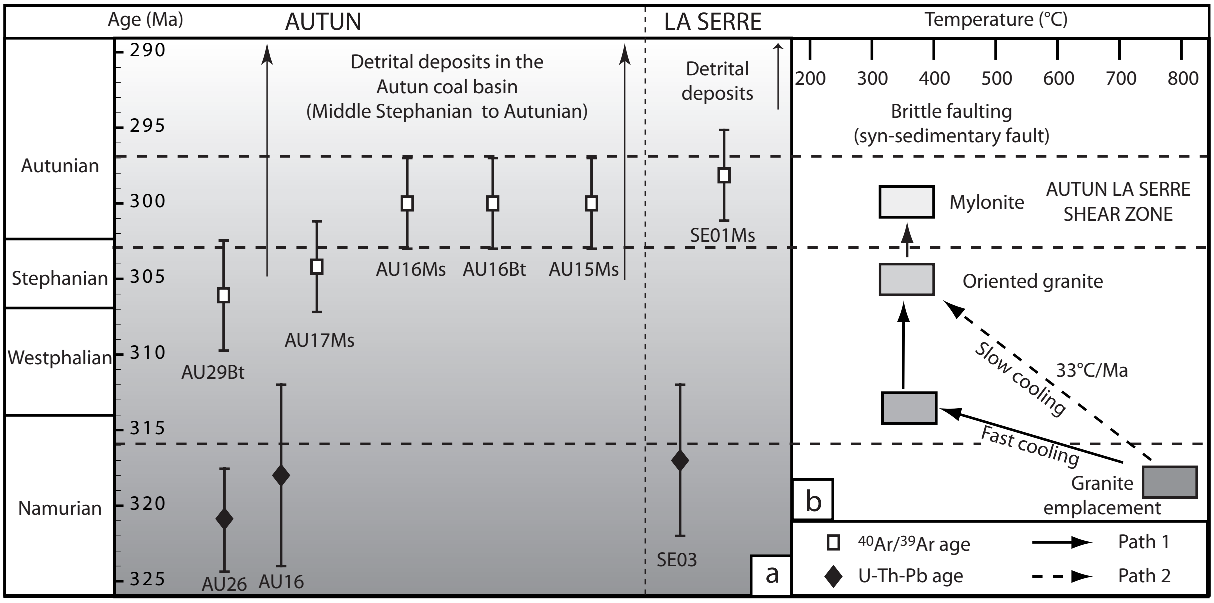
Age (Ma)
AUTUN
LA SERRE
Temperature (°C)
290
295
300
305
310
315
320
325
Autunian
Stephanian
Westphalian
Namurian
Detrital deposits in the
Autun coal basin
(Middle Stephanian to Autunian)
Detrital
deposits
AU29Bt
AU17Ms
AU16Ms
AU16Bt
AU15Ms
SE01Ms
AU26
AU16
SE03
a
200
300
400
500
600
700
800
Brittle faulting
(syn-sedimentary fault)
Mylonite
AUTUN LA SERRE
SHEAR ZONE
Oriented granite
Slow cooling
33°C/Ma
Fast cooling
Granite
emplacement
b
40Ar/39Ar age
U-Th-Pb age
Path 1
Path 2

Figure 10

Step	$^{40}Ar/^{39}Ar$	$^{38}Ar/^{39}Ar$	$^{37}Ar/^{39}Ar$	$^{36}Ar/^{39}Ar$ (.10-3)	% ^{39}Ar (released)	%$^{40}Ar^*$	$^{40}Ar^*/^{39}Ar_K$	Age (Ma)	± 1s.Ma
AU16 Bt	**J= 0.00972**								
1	399.480	0.445	0.17507	1325.176	0.14	1.97	7.89	133.3	245.8
2	41.632	0.066	0.00000	83.906	1.55	40.41	16.82	273.2	6.8
3	21.224	0.049	0.00000	14.202	4.40	80.15	17.01	276.1	2.2
4	19.546	0.047	0.00534	4.308	7.48	93.41	18.26	294.7	1.9
5	19.494	0.046	0.00863	5.695	9.78	91.29	17.80	287.8	2.0
6	19.191	0.048	0.02039	4.814	13.30	92.51	17.75	287.2	1.5
7	19.293	0.048	0.00389	1.020	15.21	98.36	18.98	305.4	2.9
8	18.948	0.043	0.01477	1.327	21.21	97.85	18.54	298.9	1.3
9	18.950	0.046	0.01560	1.710	25.47	97.26	18.43	297.3	1.5
10	18.805	0.046	0.00000	0.673	29.81	98.86	18.59	299.7	2.1
11	18.752	0.045	0.00638	0.390	39.11	99.31	18.62	300.1	1.0
12	18.791	0.047	0.00277	0.474	56.57	99.17	18.64	300.3	0.9
13	18.850	0.047	0.01177	1.291	61.99	97.90	18.45	297.6	1.8
14	19.055	0.046	0.00475	1.585	88.51	97.46	18.57	299.4	0.8
15	18.975	0.046	0.00000	0.194	94.26	99.62	18.90	304.3	1.4
16	19.063	0.046	0.00000	0.700	97.91	98.83	18.84	303.4	1.6
17	19.574	0.047	0.00000	0.720	100.00	98.83	19.35	310.9	2.3
									Total age : 298.3 +/- 2.8
AU16 Ms	**J= 0.00972**								
1	23.566	0.069	0.00000	0.075	0.25	99.84	23.53	371.6	45.7
2	18.772	0.014	0.00250	0.546	35.86	99.06	18.60	299.7	0.7
3	18.684	0.012	0.01567	0.163	50.60	99.66	18.62	300.1	0.9
4	18.843	0.013	0.01452	0.889	56.81	98.53	18.57	299.3	2.0
5	18.863	0.014	0.02630	0.578	63.66	99.02	18.68	301.0	2.0
6	19.147	0.014	0.00431	2.317	69.31	96.34	18.45	297.5	2.3
7	18.625	0.013	0.00419	0.259	80.61	99.51	18.53	298.8	1.7
8	18.504	0.013	0.00000	1.681	83.95	97.23	17.99	290.7	3.3
9	18.678	0.003	0.01472	0.000	85.22	99.92	18.66	300.8	2.8
10	18.634	0.012	0.00000	0.584	100.00	98.99	18.45	297.5	1.3
									Total age : 299.4 +/- 2.8
AU17 Ms	**J= 0.00972**								
1	63.087	0.132	0.00000	137.842	0.10	35.41	22.34	354.5	66.6
2	29.948	0.066	0.01518	37.907	0.45	62.55	18.73	301.8	17.8
3	22.628	0.019	0.00000	5.901	1.49	92.22	20.87	333.2	6.7
4	20.199	0.017	0.02163	14.006	2.35	79.44	16.05	261.5	8.1
5	19.184	0.013	0.01127	1.886	10.05	97.02	18.61	300.0	1.4
6	19.012	0.013	0.00000	0.118	18.61	99.73	18.96	305.2	1.8
7	18.909	0.012	0.00281	0.067	33.30	99.81	18.87	303.9	1.2
8	18.870	0.012	0.01473	0.000	44.22	99.92	18.86	303.6	1.0
9	18.957	0.012	0.00613	0.109	59.29	99.75	18.91	304.4	0.8
10	18.870	0.013	0.00052	0.066	87.68	99.81	18.83	303.3	1.1
11	18.562	0.012	0.01037	0.000	95.50	99.92	18.55	299.0	1.1
12	18.479	0.014	0.03320	3.118	98.19	94.94	17.54	284.1	3.0
13	18.932	0.010	0.05406	1.659	100.00	97.35	18.43	297.3	3.5
									Total age : 302.7 +/- 2.8
AU15 Bt	**J= 0.00972**								
1	21.501	0.015	1.18856	27.782	0.13	62.16	13.38	220.5	90.9
2	19.145	0.041	0.05400	9.726	2.15	84.93	16.26	264.7	6.0
3	19.269	0.037	0.00664	3.948	13.87	93.87	18.09	292.2	1.5
4	18.885	0.035	0.00736	2.429	22.29	96.12	18.15	293.2	1.7
5	18.748	0.036	0.01071	1.690	31.10	97.26	18.23	294.4	1.7
6	18.852	0.036	0.00534	0.996	50.01	98.36	18.54	299.0	1.0
7	19.063	0.038	0.00109	1.879	59.99	97.01	18.49	298.2	1.5
8	18.920	0.036	0.01655	2.516	67.57	95.99	18.16	293.3	2.5
9	18.689	0.038	0.07582	3.505	69.79	94.41	17.64	285.6	5.9
10	19.079	0.037	0.00000	0.792	82.82	98.69	18.83	303.2	1.4
11	19.578	0.039	0.00000	2.653	87.58	95.92	18.78	302.5	3.3
12	18.997	0.035	0.02738	2.098	94.66	96.66	18.36	296.3	2.1
13	19.586	0.044	0.00000	20.784	97.05	68.56	13.43	221.3	6.5
14	19.553	0.039	0.00000	11.124	100.00	83.11	16.25	264.6	4.6
									Total age : 293.6 +/- 2.8
AU15 Ms	**J= 0.00972**								
1	36.742	0.213	1.22569	113.397	0.16	9.01	3.31	57.2	95.9
2	21.106	0.021	0.40918	15.991	0.66	77.68	16.40	266.8	26.7
3	23.784	0.017	0.07458	21.037	3.42	73.82	17.56	284.3	6.7
4	20.026	0.015	0.01079	3.908	6.21	94.16	18.86	303.6	6.0
5	19.572	0.015	0.02945	3.655	12.78	94.41	18.48	298.0	2.3
6	19.078	0.013	0.00000	1.033	19.06	98.32	18.76	302.1	2.3
7	18.650	0.013	0.00062	0.200	61.87	99.60	18.58	299.4	1.0
8	19.113	0.012	0.00000	2.759	66.01	95.65	18.28	295.1	3.6
9	19.001	0.013	0.00000	1.427	71.11	97.70	18.56	299.3	3.1
10	18.814	0.013	0.00000	0.055	83.55	99.83	18.78	302.5	1.3
11	18.971	0.011	0.00994	2.316	86.61	96.31	18.27	294.9	4.8
12	19.166	0.014	0.00750	2.619	89.00	95.88	18.38	296.5	5.8
13	18.540	0.006	0.00000	0.000	89.99	99.92	18.52	298.7	3.8
14	18.835	0.011	0.00000	1.111	100.00	98.17	18.49	298.2	1.7
									Total age : 298.7 +/- 2.8
SE01 Ms	**J= 0.009621**								
1	20.815	0.020	0.00000	1.879	3.57	97.26	20.24	321.0	8.5
2	19.549	0.014	0.00000	0.000	6.77	99.92	19.53	310.7	1.4
3	19.007	0.010	0.00000	0.033	25.36	99.87	18.98	302.6	2.2
4	18.779	0.009	0.00000	0.000	48.12	99.92	18.76	299.4	0.8
5	18.673	0.009	0.00000	0.000	64.81	99.92	18.66	297.8	1.9
6	18.557	0.012	0.00000	0.002	74.58	99.91	18.54	296.1	2.3
7	18.449	0.006	0.02845	1.287	80.28	97.87	18.06	289.0	5.5
8	18.585	0.006	0.02262	0.000	91.42	99.92	18.57	296.6	0.9
9	18.643	0.005	0.01161	0.000	100	99.92	18.63	297.4	1.0
									Total age : 299.6 +/- 2.9
AU29 Bt	**J= 0.009621**								
1.00000	21.229	0.03600	0.00000	8.368	9.95000	88.28000	18.74000	299.06900	2.43500
2.00000	20.064	0.03300	0.00000	4.940	16.00000	92.65000	18.59000	296.82900	3.69700
3.00000	19.688	0.03300	0.00273	0.725	29.28000	98.83000	19.46000	309.58100	2.26800
4.00000	19.364	0.03100	0.03638	0.000	34.93000	99.92000	19.35000	308.02000	1.33700
5.00000	19.627	0.03200	0.00596	1.585	41.60000	97.54000	19.14000	304.98300	2.29300
6.00000	19.629	0.03300	0.00000	1.820	48.66000	97.18000	19.08000	303.98800	2.04600
7.00000	19.410	0.03200	0.00708	0.459	55.11000	99.22000	19.26000	306.67000	2.76900
8.00000	19.450	0.03300	0.00363	0.672	73.11000	98.90000	19.24000	306.33800	1.78700
9.00000	19.626	0.03200	0.00000	1.158	80.33000	98.18000	19.27000	306.80400	2.25700
10.00000	19.718	0.03300	0.01081	1.587	88.44000	97.55000	19.23000	306.31700	2.13500
11.00000	19.306	0.03200	0.00269	0.088	100.00000	99.79000	19.26000	306.74900	2.82400
									Total age : 305.6 +/- 2.9